GeroScience (2024) 46:3779–3800
https://doi.org/10.1007/s11357-024-01074-7

ORIGINAL ARTICLE

Effect of high-fat diet on cerebral pathological changes of cerebral small vessel disease in SHR/SP rats

Yuchi Zhang · Abdullah Md. Sheikh · Shatera Tabassum · Kenichi Iwasa · Abu Zaffar Shibly · Xiaojing Zhou · Ruochen Wang · Jubo Bhuiya · Fatema Binte Abdullah · Shozo Yano · Yoshihito Aoki · Atsushi Nagai

Received: 24 September 2023 / Accepted: 10 January 2024 / Published online: 6 February 2024

Abstract Cerebral small vessel diseases (CSVD) are neurological disorders associated with microvessels, manifested pathologically as white matter (WM) changes and cortical microbleeds, with hypertension as a risk factor. Additionally, a high-fat diet (HFD) can affect peripheral vessel health. Our study explored how HFD affects cerebral small vessels in normotensive WKY, hypertensive SHR, and SHR/SP rats. The MRI results revealed that HFD specifically increased WM hyperintensity in SHR/SP rats. Pathologically, it increased WM pallor and vacuolation in SHR and SHR/SP rats. Levels of blood–brain barrier (BBB) protein claudin 5 were decreased in SHR and SHR/SP compared to WKY, with HFD having minimal impact on these levels. Conversely, collagen IV levels remained consistent among the rat strains, which were increased by HFD. Consequently, HFD caused vessel leakage in all rat strains, particularly within the corpus callosum of SHR/SP rats. To understand the underlying mechanisms, we assessed the levels of hypoxia-inducible factor-1α (HIF-1α), Gp91-phox, and neuroinflammatory markers astrocytes, and microglia were increased in SHR and SHR/

Supplementary Information The online version contains supplementary material available at https://doi.org/10.1007/s11357-024-01074-7.

Y. Zhang · K. Iwasa · A. Z. Shibly · X. Zhou · R. Wang · J. Bhuiya · F. B. Abdullah · Y. Aoki · A. Nagai (✉)
Department of Neurology, Faculty of Medicine, Shimane University, 89-1 Enya-Cho, Izumo 693-8501, Japan
e-mail: anagai@med.shimane-u.ac.jp

Y. Zhang
e-mail: zhangyuchi1014@icloud.com

K. Iwasa
e-mail: ken1wasa@med.shimane-u.ac.jp

A. Z. Shibly
e-mail: zaffarshibly1987@gmail.com

X. Zhou
e-mail: zxjccx315@163.com

R. Wang
e-mail: m239606@med.shimane-u.ac.jp

J. Bhuiya
e-mail: m239427@med.shimane-u.ac.jp

F. B. Abdullah
e-mail: m239401@med.shimane-u.ac.jp

Y. Aoki
e-mail: yaoki@med.shimane-u.ac.jp

Y. Zhang
Department of Pharmacology, School of Basic Medical Sciences, Heilongjiang University of Chinese Medicine, Harbin 150040, China

A. M. Sheikh · S. Tabassum · S. Yano
Department of Laboratory Medicine, Faculty of Medicine, Shimane University, Izumo 693-8501, Japan
e-mail: abdullah@med.shimane-u.ac.jp

S. Tabassum
e-mail: tabassum@med.shimane-u.ac.jp

S. Yano
e-mail: syano@med.shimane-u.ac.jp

SP compared to WKY and were further elevated by HFD in all rat strains. Gp91-phox was also increased in SHR and SHR/SP compared to WKY, with HFD causing an increase in WKY but little effect in SHR and SHR/SP. In conclusion, our study demonstrates that HFD, in combined with hypertension, intensifies cerebral pathological alterations in CSVD rats. This exacerbation involves increased oxidative stress and HIF-1α in cerebral vessels, triggering neuroinflammation, vascular basement membrane remodeling, IgG leakage, and ultimately WM damage.

Keywords Cerebral small vessel disease (CSVD) · White matter (WM) · High-fat diet (HFD) · SHR · SHR/SP · Blood–brain barrier (BBB)

Introduction

Cerebral small vessel diseases (CSVD) encompass a variety of chronic neurological conditions resulting from damage to the small vessels in the cortex, white matter (WM), and subcortical areas of the brain [1–3]. Clinically, CSVD can manifest in various ways including lacunar strokes, intracerebral hemorrhages, and observable WM alterations on MRI scans [4]. The symptoms of CSVD are diverse and depend on the location and extent of brain damage, including cognitive impairment, executive dysfunction, gait disturbances, mood changes, and focal neurological deficits such as weakness or sensory loss [5]. Pathologically, CSVD comprises several distinct types, among them are arteriosclerosis, cerebral amyloid angiopathy (CAA), genetic CSVDs (like CADASIL and CARASIL), inflammatory variations, and other subtypes [1]. Among these types, arteriosclerosis is most prevalent in the elderly population. It is characterized by sclerotic changes in small vessel walls leading to impaired autoregulation and reduced perfusion of cortical and WM areas [1]. However, the comprehensive molecular mechanisms underlying these vascular changes remain incompletely elucidated.

Hypertension is recognized as the primary cause of CSVD [6, 7]. Other risk factors for vascular diseases, including dyslipidemia, diabetes, smoking, and stressful lifestyles, are also associated with CSVD [8]. In hypertensive CSVD, there is evidence of hyaline thickening of the vessel wall due to the deposition of fibro-hyaline materials and collagens, loss of smooth muscle cells from the tunica media, degeneration of the internal elastic lamina, proliferation of fibroblasts, and deposition of hyaline materials [9]. These changes lead to thickening and increased hardness of the vessel wall. Furthermore, CSVD is associated with impaired blood–brain barrier (BBB) function, which contributes to increased perivascular spaces, hemorrhage, small vessel occlusion, reduced cerebral blood flow (CBF), and chronic cerebral hypoperfusion [9]. The pieces of evidence suggested that long-term hypertension-induced damage to vessels, particularly endothelial cells, can create a hypoxic condition, leading to the activation of hypoxia-inducible factor 1α (HIF-1α) and several inflammatory cytokines and proteases, and promoting a neuroinflammatory condition [9]. In particular, HIF-1α induces vascular endothelial growth factor, and along with the action of matrix metalloproteases, it can induce pathological angiogenesis and breakdown of the BBB [9]. Metalloproteases are also responsible for the degradation of vessel basement membranes, as evidenced by decreased collagen IV, which is frequently observed in CSVD [10]. Moreover, reactive oxygen species (ROS) are known to induce BBB disturbances, endothelial dysfunction, and vascular degeneration, which are commonly seen in CSVD [11]. Amidst this intricate interplay, tight junctions (TJs) exclusive to brain endothelial cells, play a pivotal role in sealing the BBB, with claudin subtypes 1, 3, 5, and 12 expressed at endothelial TJs, with claudin 5, in particular, forming a significant component of the BBB [12, 13]. This orchestrated interplay, encompassing HIF-1α, collagen IV, ROS, and tight junction proteins, constitutes the complex symphony behind BBB disruption in CSVD. This deep comprehension guides our exploration of CSVD's intricate pathogenesis and potential other risk factors.

Nowadays, hypertension is frequently found to be accompanied by dyslipidemia, diabetes, and obesity. Dyslipidemia, diabetes, and obesity independently

A. Z. Shibly
Department of Biotechnology and Genetic Engineering, Mawlana Bhashani Science and Technology University, Santosh, Tangail 1902, Bangladesh

X. Zhou
Department of Neurology, Zhoushan Hospital, Zhoushan 316004, China

contribute to the risk of vascular diseases, including CSVD [14–17]. The primary factor underlying these conditions is believed to be the adoption of a Western-style diet, characterized by a high content of saturated fat [18, 19]. On the other hand, obesity-induced CSVD often exhibits lacunae without prominent white matter hyperintensities (WMH), in contrast to hypertension-induced CSVD [14]. Therefore, hypertension, obesity, and dyslipidemia are risk factors for CSVD with varying impacts. They often occur together, making it important to comprehend their interactions. However, the exact connection between these factors and the molecular changes in CSVD is not well-known. In this study, we hypothesized that a combination of risk factors such as hypertension and high-fat diet (HFD) might exacerbate CSVD by affecting different aspects of the pathology compared to a single risk factor. To investigate the interplay of these risk factors at the molecular pathology level, we devised a study wherein a hypertensive CSVD model was exposed to HFD. Subsequently, we meticulously analyzed alterations in cerebral small vessels at the molecular pathology level.

There are limited animal models of CSVD available. Besides specific genetic knockout models, the two most commonly used animal models that have been demonstrated to mimic CSVD are the bilateral common carotid artery occlusion (BCCAO) model and other genetically predisposed models such as spontaneously hypertensive/stroke-prone (SHR/SP) rats [20]. In the BCCAO model, hypo-perfusion is induced by permanently ligating both common carotid arteries, and subsequent brain changes are studied. While this model can explain large vessel occlusion-induced hypo-perfusion and related brain tissue changes, it may not fully capture hypertension-induced changes in cerebral small vessels. On the other hand, the SHR/SP model establishes vessel changes after the development of hypertension, making it a more suitable model for studying hypertension-induced CSVD. This model exhibits small vessel sclerosis, BBB changes, and vessel degeneration, all of which are hallmarks of CSVD. In addition to the SHR/SP rats, we also used stroke-resistant spontaneous hypertensive rats (SHR), which show only little vessel changes even after developing hypertension [19]. Notably, SHR, SHR/SP model males have a higher incidence of blood pressure and stroke than females of the same strain [21, 22]. Therefore, we chose male SHR/SP rats as the CSVD animal model for our experiments. We included normotensive male Wistar-Kyoto rats (WKY) in our study to assess the independent effects of HFD on CSVD. Our findings indicate that HFD does indeed increase CSVD in a hypertension-independent manner. Thus, our study not only demonstrated that HFD can contribute to cerebrovascular disease, but also emphasized their role in exacerbating the disease process in conditions without hypertension, providing a sound scientific basis for further treatment and intervention.

Materials and Methods

Animals

Male spontaneously hypertensive rats (SHR) and spontaneously hypertensive/ stroke-prone rats (SHR/SP) were used as CSVD models and Wistar-Kyoto (WKY) rats as a control. The WKY, SHR, and SHR/SP rats for this experiment were obtained by self-mating through the Department of Experimental Animals, Interdisciplinary Center for Science Research, Shimane University, with the approval of the Ethics Committee of Shimane University (approval number: IZ31-71). The animals were provided with free access to food and water at a controlled temperature (23 ± 2 °C) and with a 12-h light cycle (lights came on at 7:00 a.m.). All animals were used according to the ARRIVE reporting guidelines (Animal Research: Reporting of In Vivo Experiments), and guidelines of the Institute of Experimental Animals of Shimane University. The experimental protocols and procedures were approved by the Ethical Committee of Shimane University (approval code: IZ2-96).

Experimental Design

As shown in Fig. 1 (created in BioRender.com), to investigate the impact of the HFD on cerebral pathological changes of WKY, SHR, and SHR/SP rats, we used 12-week-old WKY, SHR, and SHR/SP rats divided fed 8 weeks with a normal diet (ND) or with HFD (60% lard). They were then divided into 6 experimental groups, including the ND groups (ND-WKY, ND-SHR, and ND-SHR/SP) and the HFD groups (HFD-WKY, HFD-SHR, and HFD-SHR/SP), with approximately 8 rats in each group, totaling 48

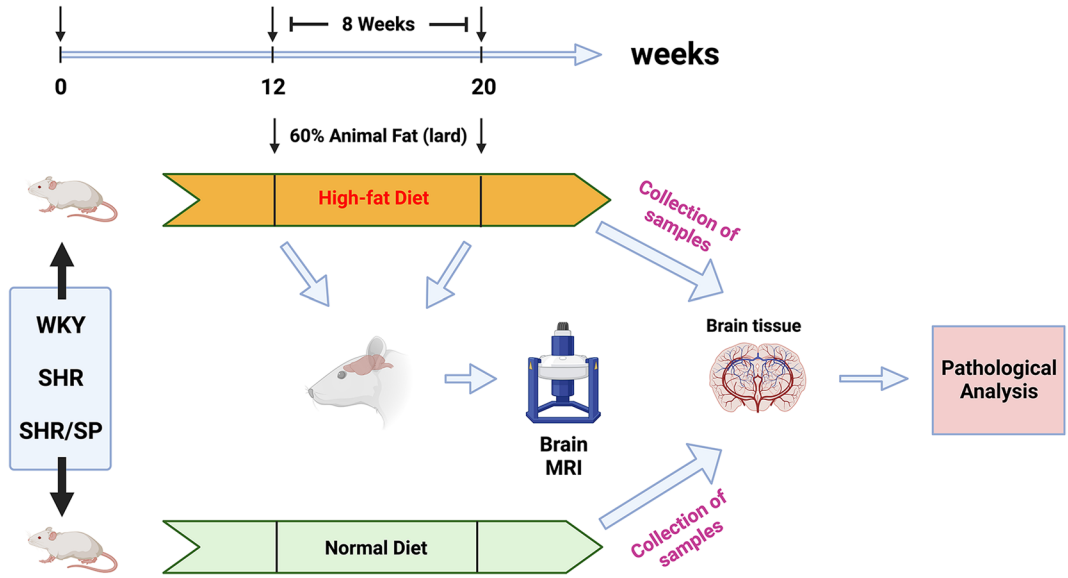

Fig. 1 Experimental design. 12-week-old WKY, SHR, and SHR/SP rats were divided them into a high-fat diet group (HFD-WKY, HFD-SHR, and HFD-SHR/SP) and a normal diet group (ND-WKY, ND-SHR, and ND-SHR/SP). The high-fat diet (HFD) group was fed a diet containing 60% lard for 8 weeks, while the normal diet (ND) group was fed a normal diet for 8 weeks. Blood pressure and MRI were measured before and after 8 weeks of HFD feeding in the HFD group, and the body weight of each rat in each group was measured weekly. After 8 weeks of feeding, brain tissues were taken from all groups of rats to observe pathological changes

animals. The body weight of each group was measured weekly throughout the experiment. Subsequently, four rats in each of the HFD groups (HFD-WKY, HFD-SHR, and HFD-SHR/SP) were subjected to blood pressure and brain magnetic resonance imaging (MRI) before and after 8 weeks of HFD feeding, respectively. One day after the brain MRI examination, for the staining experiment, all rats were food-deprived overnight, deeply anesthetized with isoflurane, and transcranial perfused with normal saline, followed by 4% paraformaldehyde (PFA) in 100 mM phosphate-buffered saline (PBS, pH = 7.4) for tissue fixation. All tissues were removed and post-fixed into the same fixative for 24 h and were cryoprotected with 30% sucrose solution in 100 mM PBS for 48 h at 4 °C. Finally, these tissues were serially sectioned coronally into tissue blocks of 2 mm thickness, and 10 μm thickness tissue slices were prepared for staining using a cryostat (Leica, Wetzlar, Germany).

Blood pressure measurements

Blood pressure was measured before and after HFD feeding in conscious, prewarmed, restrained WKY, SHR, and SHR/SP rats (n = 4/group) by tail-cuff apparatus (BP98AL, Softron, Tokyo, Japan) following the previous procedure [23, 24]. Briefly, rats were acclimatized to restraint cages for 2 d (30 min/d) prior to the measurement of blood pressure which was taken between 09:00 and 13:00. On the day of measurement, rats were restrained, and their tails were prewarmed to 37 °C for 5 to 10 min. Then their caudal arterial pressure was measured using an oscillometric cuff connected to the apparatus positioned at the ridge of the tail. Systolic, mean, and diastolic blood pressure values were collected from each group of rats.

Magnetic resonance imaging (MRI) examination

For MRI examinations, animals were anesthetized to ensure immobilization during the imaging procedures. Anesthesia was administered in accordance with approved protocols to minimize any potential distress or discomfort experienced by the animals during the MRI scans. Inhalation anesthesia with isoflurane (Pfizer Pharmaceutical Co., Ltd, NY, USA) was administered using a vaporizer at a concentration of 1–2%, maintained throughout the MRI examination.

MRI was examined before and after HFD-WKY, HFD-SHR, and HFD-SHR/SP rats. A T2-weighted MRI image of the whole brain (n = 4/group) was acquired with a 1.5 T MRI system (Mrmini SA; DS Pharma Biomedical, Osaka, Japan). Multi-slices MRI images were obtained with NMRImager Version 3.9 readout (10 slices). We next used ImageJ analysis software version 1.53 K (NIH, Bethesda, MD, USA) to determine the hyperintensity area responsible for the lesion and measured the maximum area of the lesion on the T2-weighted images.

Kluver Barrera (KB) staining

WM integrity and myelin changes in the corpus callosum of the rat brain were examined using KB staining on the 4th coronal section of the brain (S4: interaural 7.20 mm; Bregma -1.80 mm) in each group (n = 3/group). After 20 min of air-drying at room temperature, the brain slices were incubated in 0.1% Luxol Fast Blue solution for 2 h at 56 °C, then washed successively in ethanol, 0.05% lithium carbonate, and deionized water. After the 4 min incubation at 37 °C in 0.1% cresyl violet acetate solution, the slices were washed in ethanol at 4 °C, and covered with a mounting medium [25]. Then photomicrographs were taken at a magnification of × 400 within the field of view (FOV) in the corpus callosum region of each rat under an optical microscope (NIKON ECLIPSE Ci, Nikon Co. Ltd., Tokyo, Japan). In addition, the myelin integrity of the corpus callosum using a scoring system: 0 (dense myelin), 1 (myelin pallor), 2 (non-confluent vacuoles), and 3 (confluent vacuoles) (Fig. S1) [26]. The scores of each rat were examined by two independent blinded observers. The results of the scores were averaged between the two observers.

Immunofluorescent (IF) staining

The procedure and protocol for IF staining have been reported in our previous studies [27, 28] and this study was performed on 10 µm frozen sections.

Antibodies

Antibodies reactive for the following antigens were used in this study: Solanum tuberosum lectin (STL, 1:200, Vector Laboratories, Newark, CA, USA), anti-Collagen IV IgG (rabbit polyclonal, 1:200, Novus Bio Co. Ltd., Colorado Spring, CO, USA), anti-Claudin 5 IgG (rabbit polyclonal, 1:200, Abcam Co. Ltd., Cambridge, UK), anti-Iba-1 IgG (rabbit polyclonal, 1:200, Abcam Co. Ltd., Cambridge, UK), anti-GFAP IgG (rabbit polyclonal, no dilution, Dako, Agilent Co. Ltd., Carpinteria, CA, USA), anti-GP91-phox IgG (mouse monoclonal, 1:200, Santa Cruz Biotechnology, Inc., Dallas, TX, USA) and anti-HIF-1α IgG (mouse monoclonal, 1:50, Santa Cruz Biotechnology, Inc., Dallas, TX, USA). Secondary antibodies used (all at 1:500) included Cy3-conjugated anti-rat (Sigma-Aldrich, St. Louis, MO, USA), Alexa Fluor 568-conjugated anti-mouse (Abcam Co. Ltd., Cambridge, UK), goat anti-rabbit IgG FITC (Abcam Co. Ltd., Cambridge, UK), and Alexa Fluor 594-conjugated anti-rabbit (Abcam Co. Ltd., Cambridge, UK). Hoechst 33,258 (10 µg/mL, Sigma-Aldrich, St. Louis, MO, USA) was used to identify the nuclei of the cells. At last, the slices were mounted with Ultramount (Dako, Agilent Co. Ltd., Santa Clara, CA, USA).

Image analysis

Photomicrographs of the frontal cortex, corpus callosum, and striatum regions in the brain were taken at a magnification of × 200 or × 400 within the field of view (FOV) in the same plane of each hemisphere with a fluorescence microscope (NIKON ECLIPSE 80i, Nikon Co. Ltd., Tokyo, Japan) or confocal microscopy (FV3000, Olympus Co., Ltd, Tokyo, Japan). For each antigen in all analyses, images of at least three randomly selected FOV were taken per tissue section, then the total of vessel number or positive cells or immunoreactive area or immunoreactive intensity of each FOV was measured by ImageJ analysis software version 1.53 K (NIH, Bethesda, MD, USA) and analyzed to calculate the mean (n = 3 / group).

In this study, microvessels were categorized based on their diameter, with capillaries defined as those with a diameter of less than 12 µm and small arterioles and venules ranging from 12 to 40 µm [29–31]. We employed low-magnification fluorescence microscopy (× 200) to capture images of regions rich in capillaries and areas containing small arterioles and venules. Subsequently, we conducted capillary counting and used high-magnification fluorescence microscopy (× 400) to obtain detailed images of individual capillaries for diameter measurements using ImageJ

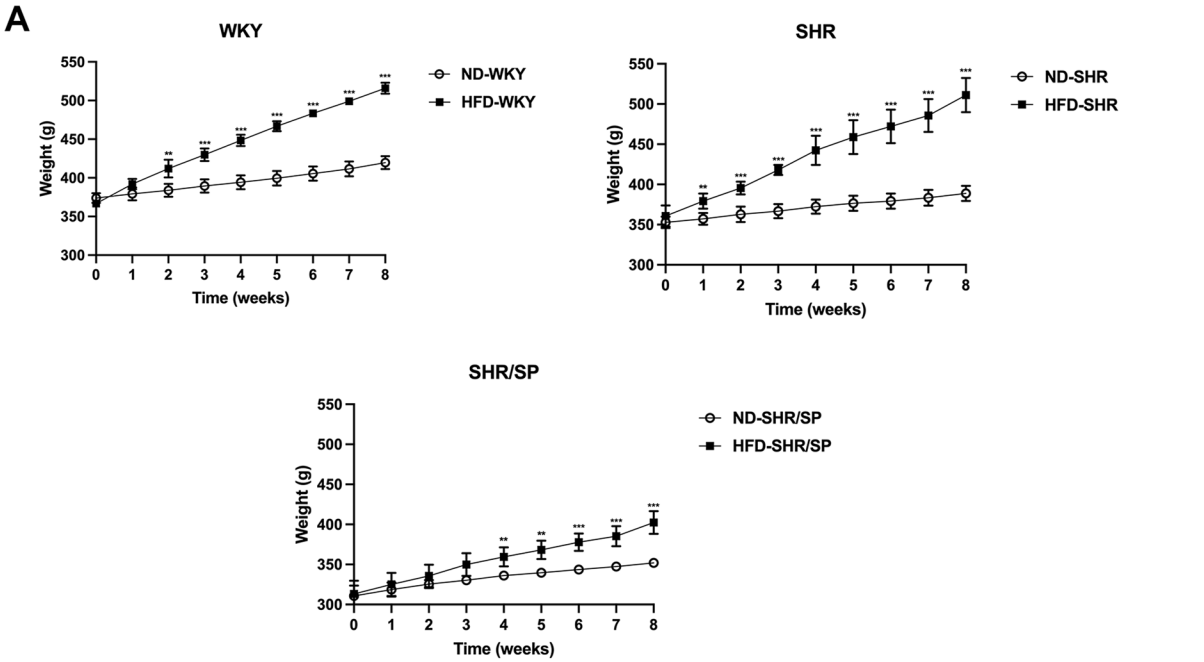
A
WKY
SHR
SHR/SP
Weight (g)
Time (weeks)
ND-WKY
HFD-WKY
ND-SHR
HFD-SHR
ND-SHR/SP
HFD-SHR/SP

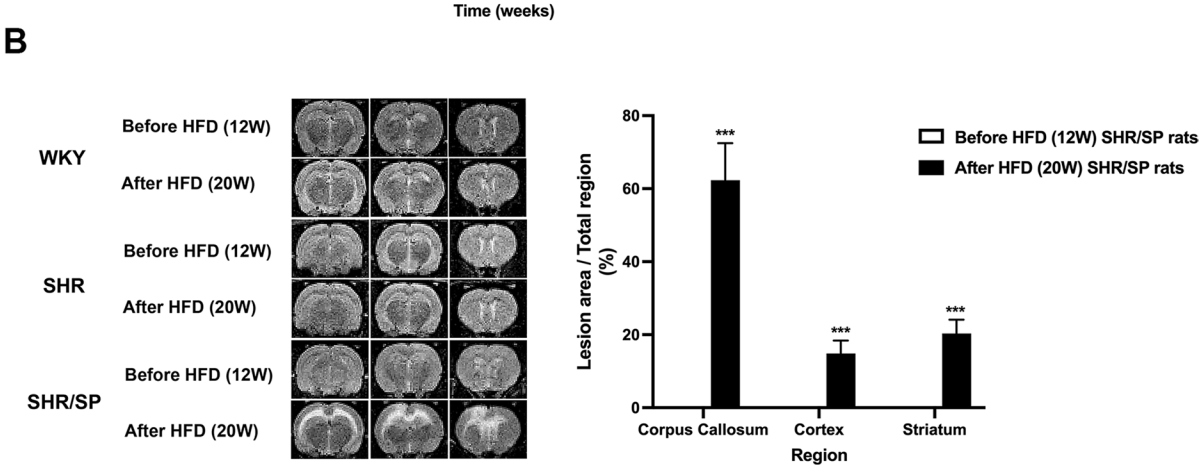
B
WKY
SHR
SHR/SP
Before HFD (12W)
After HFD (20W)
Lesion area / Total region (%)
Corpus Callosum
Cortex
Striatum
Region
Before HFD (12W) SHR/SP rats
After HFD (20W) SHR/SP rats

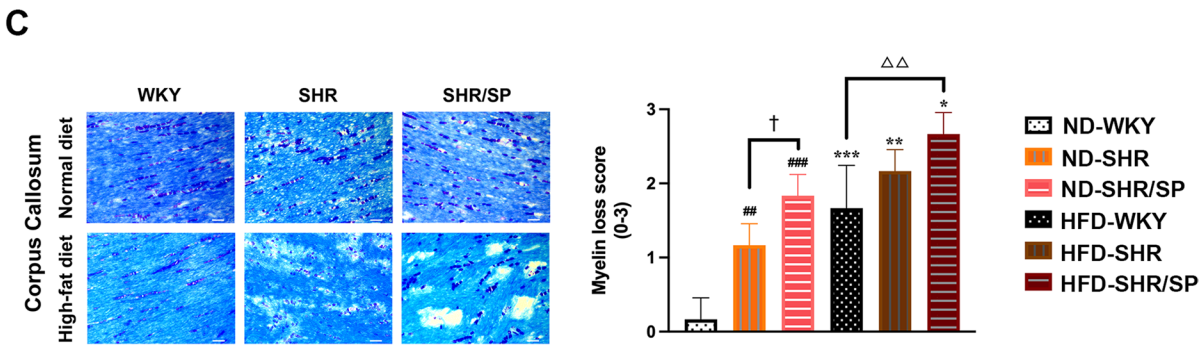
C
WKY
SHR
SHR/SP
Corpus Callosum
Normal diet
High-fat diet
Myelin loss score (0-3)
ND-WKY
ND-SHR
ND-SHR/SP
HFD-WKY
HFD-SHR
HFD-SHR/SP

◂**Fig. 2** Body weight, brain MRI, and myelin changes of WKY, SHR, and SHR/SP rats. **A** The body weights of ND-WKY, ND-SHR, ND-SHR/SP, HFD-WKY, HFD-SHR, and HFD-SHR/SP rats were measured once a week for 8 weeks starting at 12 week-age. HFD-WKY, HFD-SHR, and HFD-SHR-SP showed a significant increase in body weight compared to their corresponding ND groups. Data are summarized and presented as mean ± SD of 8 rats in each group. $^{**}P < 0.01$ and $^{***}P < 0.001$ vs. the corresponding type of ND group. **B** Brain MRI analysis of HFD-WKY, HFD-SHR, and HFD-SHR/SP rats before and after 8 weeks of HFD feeding. The images show representative serial 3-slice MRI scans of brains in coronal sections. Each section is labeled with its interaural and Bregma coordinates, providing information on its relative position within the brain. Section 3 (S3): Interaural 9.20 mm; Bregma 0.20 mm. Section 4 (S4): Interaural 7.20 mm; Bregma -1.80 mm. Section 5 (S5): Interaural 4.84 mm; Bregma -4.16 mm. The hyperintensity area was evaluated using T2-weighted MRI. After HFD feeding, only SHR/SP rats exhibited high intensity in three consecutive coronal slices (S3-S5). The high-intensity signals were primarily concentrated in the corpus callosum region, with smaller areas of high intensity observed in the frontal cortex and striatum regions. The hyperintensity volume of SHR/SP rats was calculated as the percentage of the lesion area relative to the total region in each of the three brain regions, including the cortex, corpus callosum, and striatum (%). "Before HFD (12W)" refers to the rats in the HFD group before they were fed the high-fat diet. "After HFD (20W)" refers to the rats in the HFD groups after 8 weeks of HFD feeding. The data are summarized and presented as mean ± SD of 4 rats in each group. Statistical significance is denoted as $^{***}P < 0.001$ vs. Before HFD (12W) SHR/SP rats. **C** The representative KB staining micrographs of the corpus callosum region in WKY, SHR, and SHR/SP rats after ND and HFD. Scale bar = 25 μm. The scores of each rat were examined by two independent blinded observers. The results of the scores were averaged between the two observers. The scores for WKY rats increased from 0.17 ± 0.29 (ND) to 1.67 ± 0.58 (HFD), SHR rats showed an increase from 1.17 ± 0.29 (ND) to 2.17 ± 0.29 (HFD), and SHR/SP rats exhibited an escalation from 1.83 ± 0.29 (ND) to 2.67 ± 0.29 (HFD). Results are means ± SD (n = 3). $^{*}P < 0.05$, $^{**}P < 0.01$, $^{***}P < 0.001$ vs. the corresponding results of the ND group. In the ND-fed group, $^{\#\#}P < 0.01$, $^{\#\#\#}P < 0.001$ vs. the ND-WKY rats. In the ND-fed groups, $^{\dagger}P < 0.05$ vs. the ND-SHR rats. In the HFD-fed groups, $^{\triangle\triangle}P < 0.01$ vs. the HFD-WKY rats

analysis software. Next, to assess vascular leakage, extravascular immunoglobulin G (IgG) was analyzed. STL staining was employed to distinguish vessels and identify intravascular IgG, which was then excluded from the analysis. ImageJ analysis software was also used to determine the percentage of extravascular IgG coverage in the total analyzed image area [32]. Additionally, microglial activation was quantified based on the morphological changes of the cell. Activated microglia were identified by a larger cell body and shorter processes and branches, as shown in the morphology of cells 2 and 3 in Fig. S2 [33].

Western Blotting (WB)

We collected frontal cortical brain tissues from normal diet (ND-WKY, ND-SHR, and ND-SHR/SP) and high-fat diet (HFD-WKY, HFD-SHR, and HFD-SHR/SP) rat groups and homogenized in 20-fold volume of ice-cold RIPA lysis buffer (onefold phosphate-buffered saline, pH 7.4, 1% Nonidet p-40 0.5% sodium deoxycholate, 0.1% SDS, 10 μg/mL PMSF, 10 μg/mL aprotinin). The total proteins (70 ug per lane) were subsequently separated by 10% sodium dodecyl sulfate–polyacrylamide gel electrophoresis (SDS-PAGE) and transferred to a PVDF membrane (Millipore, Billerica, MA, USA). After blocking for 1 h at room temperature, the membranes were blotted with primary antibodies including: anti-HIF-1α IgG (rabbit polyclonal, 1:2000, Santa Cruz, CA, USA), anti-claudin-5 IgG (rabbit polyclonal, 1:2000, Abcam Co. Ltd., Cambridge, UK),anti-collagen IV IgG (rabbit polyclonal, 1:500, Novus, Colorado Springs, CO, USA), anti-Gp91-phox IgG (mouse monoclonal, 1:200, Santa Cruz Biotechnology, Inc., Dallas, TX, USA) and anti-β-actin IgG (1:1000, mouse monoclonal, Santa Cruz, CA, USA) at 4 °C overnight. This was followed by incubation with infrared (IR) dye-conjugated anti-rabbit or anti-mouse IgG antibody (1:3000; LI-COR Bioscience, Lincoln, NE, USA) or horseradish peroxidase-conjugated anti-mouse IgG antibody (1:3000, Santa Cruz, CA, USA) for 1 h at room temperature. Immunoreactivity was visualized using an ECL kit and AMERSHAM Image Quant 800 detection system (GE Healthcare, Amersham, UK).

Statistical analysis

Data normality was verified through Shapiro–Wilk tests, and as the data approximated normal distribution, parametric tests were deemed appropriate. All results are represented as a mean ± SD. Statistical analysis of these results was carried out by t-test or one-way ANOVA (with LSD or Dunnett's T3 correction for comparison of multiple means). *P* values < 0.05 were considered statistically significant. All statistical analyses were done using IBM SPSS 26.0 Software and GraphPad Prism 9.

Results

Effect of high-fat diet (HFD) on body weight and blood pressure in WKY, SHR, and SHR/SP rats

Body weight was measured at 1-week intervals. The body weight of WKY, SHR, and SHR/SP rats in the ND and HFD increased gradually. However, the body weight of all 3 rat strains fed with HFD exhibited a significant increase in body weight compared to ND groups (Fig. 2A). Additionally, the rate of body weight increase of HFD-fed SHR/SP rats was decreased compared to that of HFD-fed WKY and HFD-SHR rats (Fig. S3).

Blood pressure was measured before and after feeding WKY, SHR, and SHR/SP rats in HFD groups. Before HFD feeding, systolic, diastolic, and mean blood pressure were high in both SHR and SHR/SP rats compared to WKY. After 8 weeks of HFD feeding, compared to before HFD feeding, HFD increased blood pressure in WKY rats only, but not in SHR and SHR/SP (Table 1).

Effect of HFD on brain MRI changes in WKY, SHR, and SHR/SP rats

To check the effects of HFD on the brain, a T2-weighted MRI was performed before and after feeding HFD to WKY, SHR, and SHR/SP rats (Fig. 2B). Before HFD feeding, there were no hyperintense regions found in WKY, SHR, and SHR/SP rats. Following HFD feeding, only SHR/SP rats exhibited WMH. Small areas of hyperintensity were also observed in the frontal cortex and striatum regions. Further analysis of the ratio of the hyperintense area revealed that about $62.25 \pm 10.16\%$ of the corpus callosum, $14.82 \pm 3.52\%$ of the cortex, and $20.28 \pm 3.76\%$ of striatum areas showed hyperintensity.

Effect of HFD on myelin in the cerebral corpus callosum region of WKY, SHR, and SHR/SP rats

To investigate further WM pathology, myelin changes were evaluated by KB staining (Fig. 2C). The myelin changes were quantified using a grading system. Results revealed that the WM of the ND-fed WKY rats displayed densely packed elongated parallel nerve fibers with almost no vacuolation. In the case of ND-fed SHR rats, slight myelin pallor was observed, whereas ND-fed SHR/SP rats exhibited both parlor and vacuolation. HFD feeding caused myelin pallor in WKY rats and myelin pallor with vacuolation in SHR rats. Especially, in the SHR/SP rats, HFD feeding caused a severe myelin parlor and increased vacuolation. Scoring of the myelin changes also showed that HFD increased myelin pathology in all rat strains (WKY = ND, 0.17 ± 0.29 vs HFD, 1.67 ± 0.58; SHR = ND, 1.17 ± 0.29 vs HFD, 2.17 ± 0.29; SHR/SP = ND, 1.83 ± 0.29 vs HFD, 2.67 ± 0.29).

Effects of HFD on cerebral small vessel density and diameter in WKY, SHR, and SHR/SP rats

Cerebral vessels were visualized using Solanum Tuberosum Lectin (STL) staining (Fig. 3A, Fig. S4). Compared with ND-fed WKY, only the corpus callosum region of ND-fed SHR rats had an increased microvessel density, and there were no significant differences in the other regions of ND-fed SHR rats or in all regions of ND-fed SHR/SP. The frontal cortex region demonstrated a significant increase in microvessel density in HFD-fed WKY, HFD-fed SHR, and HFD-fed SHR/SP rats compared to their

Table 1 Blood pressures in the WKY, SHR, and SHR/SP rats before and after HFD ($\overline{X} \pm$ SD, mmHg)

Group	Before HFD (12W)			After HFD (20W)		
	WKY	SHR	SHR/SP	WKY	SHR	SHR/SP
Systolic	128.45 ± 4.08	$173.25 \pm 15.54^{\#}$	$213.95 \pm 28.69^{\#\#\#, \dagger}$	$178.1 \pm 47.71^{**}$	182.38 ± 8.18	$208.75 \pm 7.09^{\wedge}$
Mean	105.55 ± 2.56	$147.65 \pm 12.01^{\#\#}$	$169.3 \pm 23.73^{\#}$	148.5 ± 40.82	151.45 ± 11.29	$182.3 \pm 4.94^{\wedge, \triangle}$
Diastolic	94.9 ± 4.77	$135.1 \pm 10.97^{\#\#}$	$145.05 \pm 20.57^{\#}$	140.1 ± 41.63	137.7 ± 13.26	$168.65 \pm 8.96^{\wedge}$

PS: $^{**}P < 0.01$ vs. the respective before HFD (12W). In Before HFD (12W) groups, $^{\#}P < 0.05$, $^{\#\#}P < 0.01$, $^{\#\#\#}P < 0.001$ vs. before HFD (12W) WKY rats; $^{\dagger}P < 0.05$ vs. before HFD (12W) SHR rats. In the after HFD (20W) groups, $^{\triangle}P < 0.05$ vs. the after HFD (20W) WKY rats; $^{\wedge}P < 0.05$ vs. after HFD (20W) SHR rats

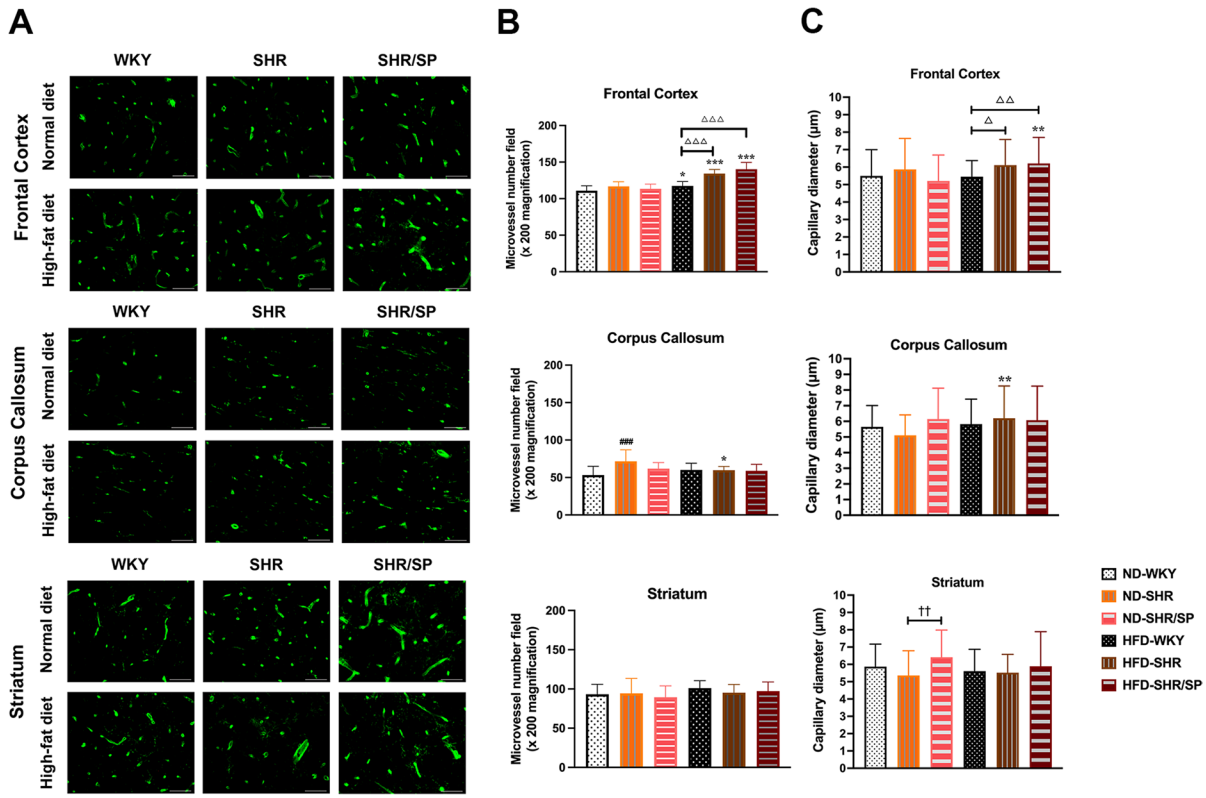

Fig. 3 HFD-induced small vessel density and diameter in the cerebral of WKY, SHR, and SHR/SP rats. **A** Cerebral vessels were revealed after Solanum Tuberosum lectin (STL) immunostaining in the frontal cortex, corpus callosum, and striatum regions of WKY, SHR, and SHR/SP rats fed ND or HFD. Scale bar = 50 μm. **B** Statistical analysis results of microvessel numbers in the frontal cortex, corpus callosum, and striatum. The microvessel density in the frontal cortex region significantly increased in HFD-WKY, HFD-SHR, and HFD-SHR/SP rats compared to their respective ND groups. **C** Statistical analysis results of capillary diameter in the frontal cortex, corpus callosum, and striatum regions. Capillary diameters in the frontal cortex were notably wider in HFD-fed SHR/SP rats compared to their ND-fed counterparts, and wider in both HFD-fed SHR and HFD-fed SHR/SP rats compared to HFD-fed WKY rats. In the corpus callosum region, capillary diameter was broader in HFD-fed SHR rats compared to ND-fed SHR rats. In the striatum region, capillary diameters were wider in ND-fed SHR/SP rats compared to ND-fed SHR rats. Results are means ± SD (n = 3, 3 FOV for each region). $^{*}P < 0.05$, $^{**}P < 0.01$, $^{***}P < 0.001$ vs. the corresponding results of the ND group. In the ND-fed group, $^{\#\#\#}P < 0.001$ vs. the ND-WKY rats. In the ND-fed group, $^{\dagger\dagger}P < 0.01$ vs. the ND-SHR rats. In the HFD-fed group, $^{\triangle}P < 0.05$, $^{\triangle\triangle}P < 0.01$, $^{\triangle\triangle\triangle}P < 0.001$ vs. the HFD-WKY rats. FOV: field of view

corresponding ND groups, with the most substantial increase observed in HFD-fed SHR and HFD-fed SHR/SP rats in comparison to HFD-fed WKY rats. In contrast, HFD-fed SHR had a lower microvessel density in the corpus callosum region compared to ND-fed SHR and all 3 rat strains fed with HFD had no changes in the striatum region (Fig. 3B, Fig. S4).

The diameter analysis revealed that in the frontal cortex region of SHR and SHR/SP, capillary diameters were increased in HFD-fed groups compared to their ND-fed counterparts (Fig. 3A, C). Also, in the corpus callosum region, the capillary diameter was increased in HFD-fed SHR rats compared to ND-fed SHR rats (Fig. 3A, C). In the striatum region, capillary diameters were increased in ND-fed SHR/SP rats compared to ND-fed SHR rats (Fig. 3A, C). Additionally, measurements of small artery and vein diameters did not yield statistically significant differences (data not shown).

HFD-induced expression of cerebral hypoxia-inducible factor-1α (HIF-1α) in WKY, SHR, and SHR/SP rats

To understand the mechanisms of increased small vessel density, we have analyzed the levels of HIF-1α (Fig. 4A, Fig. S5). Within the ND groups, HIF-1α levels were increased in SHR compared to WKY, which was further increased in SHR/SP in the frontal cortex, corpus callosum, and striatum regions. A similar trend was also observed in the HFD groups. A significant increase in HIF-1α expression was noted in the HFD groups across all regions when compared to the ND groups. Western blotting of HIF-1α using cortex tissues also showed similar results like immunostaining quantification (Fig. S9).

Double immunofluorescence staining revealed that HIF-1α was mainly positive in the blood vessels (Fig. 4B, Fig. S5-A), while a minor portion of these signals were identified in microglia (Fig. 4B, Fig. S5-B). Additionally, microglia and astrocytes were found in the vicinity of HIF-1α-positive vessels (Fig. 4B, Fig. S5-B, C).

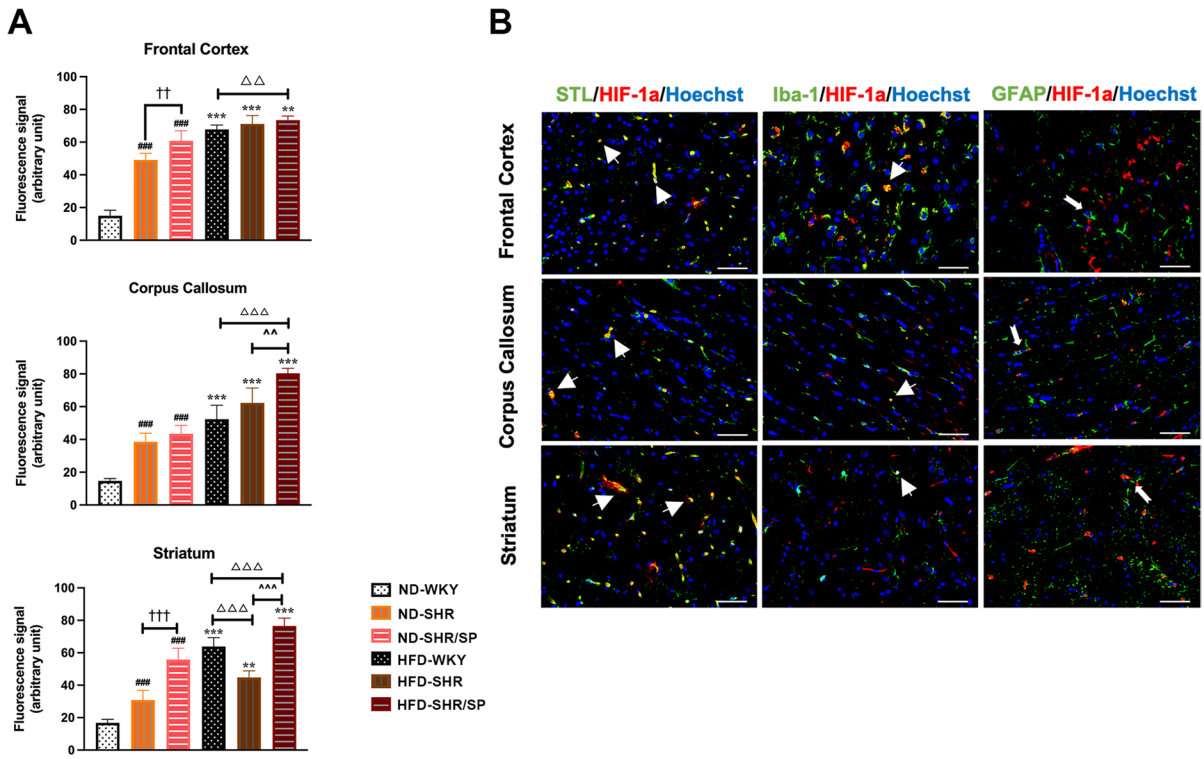

Fig. 4 HFD-induced hypoxia-inducible factor-1α (HIF-1α) expression in the WKY, SHR, and SHR/SP rats, and the localization of HIF-1α in the brain of HFD-SHR/SP rats. **A** Statistical analysis results of HIF-1α expression in the frontal cortex, corpus callosum, and striatum regions. HFD induced HIF-1α expression in the cerebral frontal cortex, corpus callosum, and striatum of WKY, SHR, and SHR/SP rats. Results are means ± SD (n = 3, 3 FOV for each region). $^{**}P < 0.01$, $^{***}P < 0.001$ vs. the corresponding results of the ND group. In the ND-fed group, $^{###}P < 0.001$ vs. the ND-WKY rats. In the ND-fed group, $^{††}P < 0.01$, $^{†††}P < 0.001$ vs. the ND-SHR rats. In the HFD-fed groups, $^{ΔΔ}P < 0.01$, $^{ΔΔΔ}P < 0.001$ vs. the HFD-WKY rats. In the HFD-fed groups, $^{^^^}P < 0.001$ vs. HFD-SHR rats. FOV: field of view. **B** The co-localization of HIF-1α in the cerebral frontal cortex, corpus callosum, and striatum of HFD-SHR/SP rats. Red fluorescent protein staining identified HIF-1α, and co-localized with vascular marker STL, microglia marker Iba-1 and astrocyte marker GFAP staining (green). Nuclei are labeled with Hoechst (blue). The figure illustrated triple immunostaining in the frontal cortex, corpus callosum, and striatum regions of HFD-SHR/SP. Triple-stained merged photographs are shown here. Scale bar = 50 μm. The yellow color indicated areas where STL and Iba-1 co-located with HIF-1α (thick arrows), while the dovetail arrows represent GFAP expression around HIF-1α

HFD-induced changes in cerebral collagen IV and claudin 5 expression in WKY, SHR, and SHR/SP rats

To evaluate the changes in the vascular basement membrane, collagen IV (Col IV) staining was done (Fig. 5A). Within the ND groups, the levels of Col IV were decreased in ND-SHR/SP compared to ND-SHR, which were further decreased compared to ND-WKY in the striatum region. In the corpus callosum region, the levels of Col IV were increased in HFD-fed WKY and SHR rats compared to their ND counterparts (Fig. 5B). Additionally, HFD increased Col IV levels in the corpus callosum and striatum regions of WKY, and also in the frontal cortex and corpus callosum regions of SHR rats. The most pronounced changes in Col IV levels were observed in SHR/SP rats, where HFD increased Col IV levels in all regions we checked compared to their ND-fed counterpart (Fig. 5B). Similarly, Western blotting of Col IV revealed similar results like immunostaining quantification in the cortex tissues (Fig. S9).

Next, we evaluated BBB protein claudin 5 levels in the vessels across the three regions by double fluorescence staining (Fig. 5C, Fig. S6). It was also quantified by Western blotting (Fig. S9). The results showed a decrease in claudin 5 levels in STL-positive vessels of ND-fed SHR in all regions, but it was more pronounced in the frontal cortex and corpus callosum regions of ND-fed SHR/SP rats as compared with their ND-fed WKY counterparts (Fig. 5D). Moreover, in WKY rats, HFD decreased claudin 5 levels in all regions (Fig. 5D). However, in SHR rats, HFD decreased claudin 5 levels only in vessels of the corpus callosum and striatum (Fig. 5D). Whereas the results of Western Blotting showed that similar results like immunostaining quantification in the cortex tissues (Fig. S9).

Effect of HFD on cerebral vascular integrity in WKY, SHR, and SHR/SP rats

The cerebrovascular integrity was evaluated by observing the extravasation of immunoglobulin G (IgG) (Fig. 6A, Fig. S7). ND-fed WKY showed no IgG extravasation, which was seen in all regions of ND-fed SHR and ND-fed SHR/SP. In WKY rats, varying degree of IgG extravasation was evident after feeding with HFD in all regions. In SHR and SHR/SP rats, IgG extravasation was increased after feeding with HFD in all regions. In the HFD groups, both HFD-fed SHR and HFD-fed SHR/SP rats displayed an augmented vascular leakage area compared to HFD-fed WKY rats, with HFD-fed SHR/SP rats showing a more substantial increase than HFD-fed SHR rats in all regions. Especially, the corpus callosum region demonstrated the most significant increase in IgG extravasation in HFD-fed SHR/SP rats (Fig. 6B).

Effects of HFD on cerebral microglia and astrocytes in WKY, SHR, and SHR/SP rats

To assess the changes in microglia and astrocytes, immunofluorescence staining of Iba-1 and GFAP was done (Figs. 7A and 8A). The morphology of Iba-1-positive microglia was evaluated to understand its activation state in the three regions (Fig. 7C). The number of activated microglia and Iba-1, GFAP-positive areas were significantly increased in ND-fed SHR and ND-fed SHR/SP rats compared to ND-fed WKY rats in all regions (Figs. 7B-C and 8B). Moreover, ND-fed SHR/SP rats displayed a further increase relative to ND-fed SHR rats. The HFD groups exhibited similar trends in all regions compared to the ND groups, with varying degrees of increase observed among HFD-fed WKY, HFD-fed SHR, and HFD-fed SHR/SP rats (Fig. 7B-C and 8B).

Effects of HFD on cerebral Gp91-phox expression in WKY, SHR, and SHR/SP rats

The impact of HFD on the levels of the oxidative stress-related protein Gp91-phox was assessed across three regions (Fig. 9A, Fig. S8). In ND-fed groups, Gp91-phox levels were increased in SHR and SHR/SP compared to WKY rats in all regions. In WKY and SHR rats, HFD increased Gp91-phox levels in all regions. In SHR/SP rats, HFD increased Gp91-phox levels in the frontal cortex and corpus callosum regions (Fig. 9A). In the Western blotting results, it was shown that similar results like immunostaining quantification in the cortex tissues (Fig. S9).

Moreover, the localization of Gp91-phox in blood vessels, microglia, and astrocytes was investigated across all regions (Fig. 9B, Fig. S8). The results indicated that the Gp91-phox positive signal was predominantly expressed in blood vessels, with minimal expression in microglia and astrocytes. Additionally,

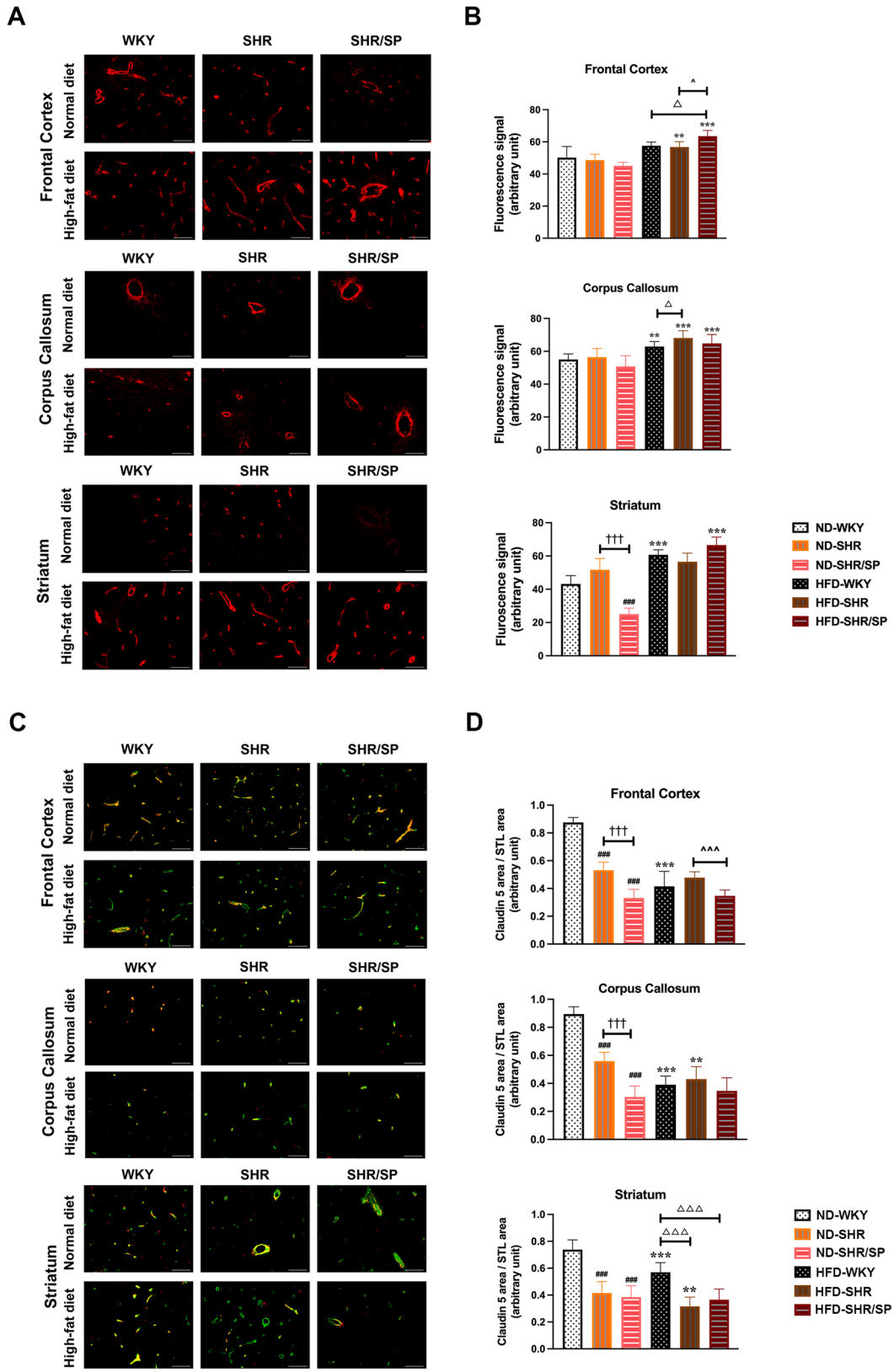
A
WKY
SHR
SHR/SP
Frontal Cortex
Normal diet
High-fat diet
Corpus Callosum
Striatum
B
Frontal Cortex
Fluorescence signal (arbitrary unit)
Corpus Callosum
Striatum
Flurescence signal (arbitrary unit)
ND-WKY
ND-SHR
ND-SHR/SP
HFD-WKY
HFD-SHR
HFD-SHR/SP
C
D
Claudin 5 area / STL area (arbitrary unit)

◂**Fig. 5** HFD-induced collagen IV and claudin 5 expression in the cerebral frontal cortex, corpus callosum, and striatum of WKY, SHR, and SHR/SP rats. **A** Cerebral vascular basement membrane was revealed after collagen IV (col IV) immunostaining in the frontal cortex, corpus callosum, and striatum of WKY, SHR, and SHR/SP rats fed ND or HFD. Scale bar = 50 μm. **B** Statistical analysis results of vascular basement membrane expression in the frontal cortex, corpus callosum, and striatum regions. Col IV expression significantly changed in the corpus callosum among HFD-fed WKY, HFD-fed SHR, and HFD-fed SHR/SP rats compared to their respective ND groups. **C** The figure illustrated dual immunostaining for the vessel marker STL (green) and tight junction protein of the BBB marker claudin 5 (red) in the frontal cortex, corpus callosum, and striatum regions of WKY, SHR, and SHR/SP rats fed ND or HFD. Dual-stained merged photographs are shown here (Scale bar = 50 μm). **D** Quantification of the claudin 5 area / STL area is shown in the frontal cortex, corpus callosum, and striatum regions. Comparing HFD groups with ND groups, claudin 5 expression in vessels decreased in HFD-WKY rats compared to ND-WKY rats in all regions, whereas HFD-SHR rats was also decreased than ND-SHR rats, particularly in the corpus callosum and striatum regions. Results are means ± SD (n = 3, 3 FOV for each region). $^{**}P < 0.01$, $^{***}P < 0.001$ vs. the corresponding results of the ND group. In the ND-fed group, $^{\#\#\#}P < 0.001$ vs. the ND-WKY rats. In the ND-fed group, $^{\dagger\dagger\dagger}P < 0.001$ vs. the ND-SHR rats. In the HFD-fed group, $^{\Delta}P < 0.05$, $^{\Delta\Delta\Delta}P < 0.001$vs. the HFD-WKY rats. In the HFD-fed group, $^{\wedge}P < 0.05$, $^{\wedge\wedge\wedge}P < 0.001$ vs. the HFD-SHR. FOV: field of view

a few microglia and astrocytes were observed surrounding the Gp91-phox positive vessels.

Discussion

The present study investigated the accumulative effect of HFD added upon hypertension overload in the CSVD pathology of SHR and SHR/SP rats. It is known that a high fat-containing diet, especially saturated fat, and hypertension can affect peripheral vessel health. In this study, we demonstrated that HFD can affect cerebral small vessels independently, and augment hypertension-induced effects causing pathological changes similar to CSVD including BBB disruption, changes of vessel basement membrane, and increased neuroinflammation. WMH in T2-weighted MRI and decreased vessel integrity are considered diagnostic features of CSVD, especially hypertension-induced CSVD in humans [7, 34, 35]. In the case of our study, HFD affects both of these features, especially in severely hypertensive SHR/SP rats. Also, pathological changes like hypertension-induced vessel leakage were increased by HFD across the different brain regions in all rat strains. Particularly, extensive vessel leakage was observed in the corpus callosum region of hypertensive SHR/SP rats fed with HFD. As a result, we observed a cumulative pathological effect of T2 WMH in the corpus callosum region of SHR/SP rats following HFD feeding, with the frontal cortex and striatum areas also showing T2 hyperintensity but to a lesser extent. Although we observed that the vessel leakage was increased in hypertensive SHR rats, we did not find WM, cortical, or striatum hyperintensity even after HFD feeding. However, the SHR/SP rats have a more pronounced degree of hypertension compared to SHR rats. This suggested the possibility that the cumulative effects of hypertension and HFD on WM changes are greater in SHR/SP causing the change visible early, while similar changes potentially develop in SHR rats at a later time. Importantly, HFD also induced leakage in normotensive WKY rats, indicating it could be an independent risk for cerebral vessels. Hence, along with hypertension, dietary interventions might also need to be considered for the management of CSVD, and overall, the health of cerebral small vessels.

In the WM areas, blood flow is lower than in cortical areas because of low energy demand. Such differences in perfusion also make WM more vulnerable to altered perfusion [36]. Hence, WM changes are a prominent feature, which is usually caused by hypoperfusion or inflammation induced by underlying causes like hypertension in CSVD patients [20, 37]. Since HFD consumption can induce vascular inflammation and remodeling, the combined effects of hypertension and HFD could exacerbate WM changes in the WM areas. A previous report on the pathology of human cadavers identified the location of WMH by MRI and observed that it was more vacuolated and immunoreactive for myelin basic protein than in normal brains [38]. Meanwhile, our results of KB staining demonstrated that HFD alone can induce WM pallor. Moreover, hypertensive rat strains showed WM pallor and small vacuolation, and the extent of damage seems to correlate with the hypertension status. Interestingly, HFD exacerbated such WM damage, which resulted in characteristic WM changes consistent with CSVD in hypertensive SHR and SHR/SP rats. Taken together, these findings suggested that each condition has an exacerbating effect on WM changes, and combining hypertension

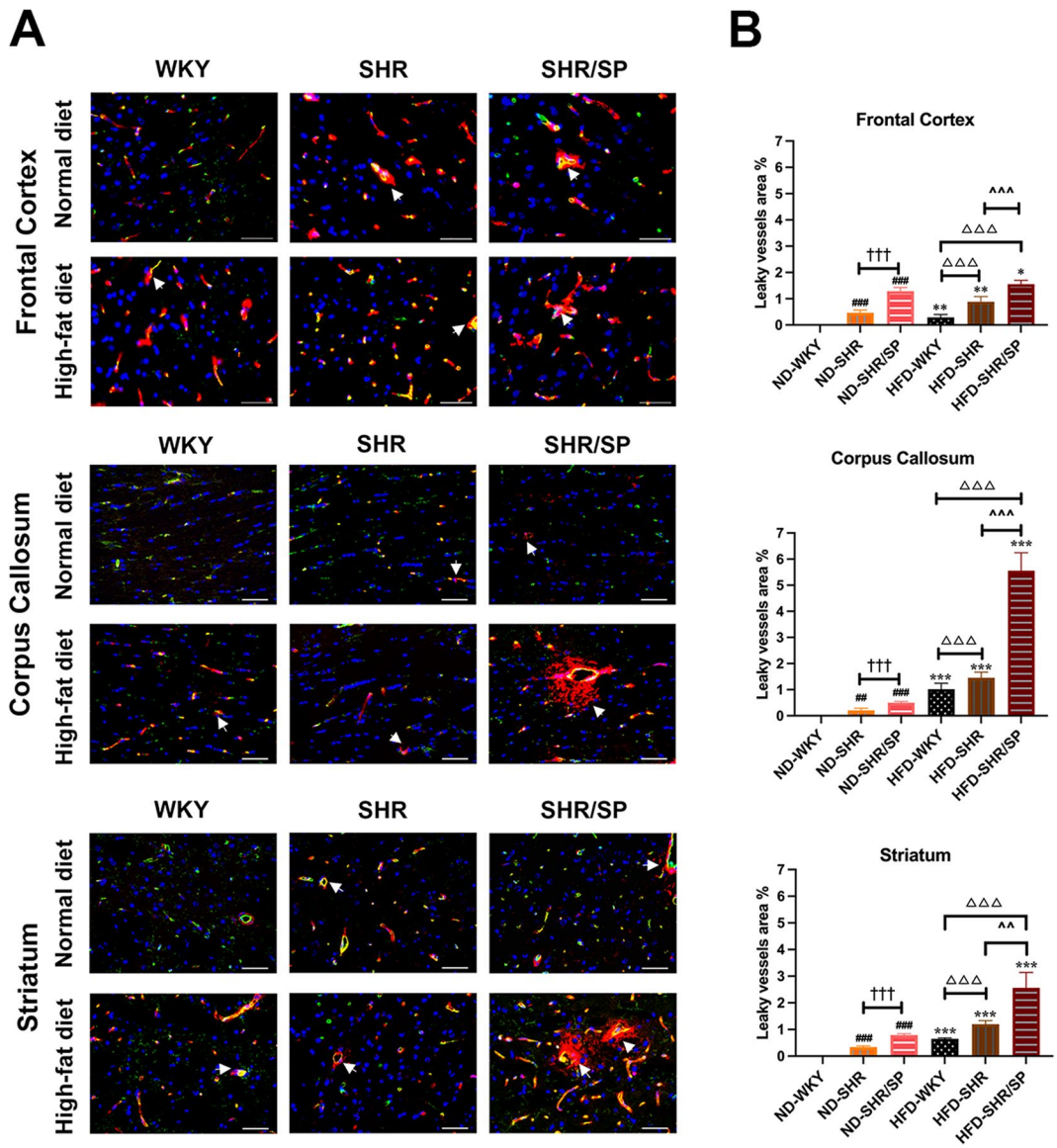

Fig. 6 HFD-induced vessel leakage in the cerebral frontal cortex, corpus callosum, and striatum of WKY, SHR, and SHR/SP rats. **A** Vessel leakage was identified by extravasation of IgG in the brain parenchyma (red), vessels were identified by STL staining (green) and nuclei were identified using Hoechst (blue) in the frontal cortex, corpus callosum, and striatum regions of WKY, SHR, and SHR/SP rats fed ND or HFD. Triple merged photographs are shown here (Arrow = vessel leakage, Scale bar = 50 µm). **B** Quantification of the total area of vascular leak in the frontal cortex, corpus callosum, and striatum. The HFD groups exhibited significantly increased vascular leakage areas compared to their respective ND groups in all regions, with the corpus callosum region showing the most significant increase in HFD-SHR/SP rats. Results are means ± SD (n = 3, 3 FOV for each region). $^{*}P < 0.05$, $^{**}P < 0.01$, $^{***}P < 0.001$ vs. the corresponding results of the ND group. In the ND-fed group, $^{\#\#}P < 0.01$, $^{\#\#\#}P < 0.001$ vs. the ND-WKY rats. In the ND-fed group, $^{\dagger\dagger\dagger}P < 0.001$ vs. the ND-SHR rats. In the HFD-fed group, $^{\Delta\Delta\Delta}P < 0.001$ vs. the HFD-WKY rats. In the HFD-fed group, $^{\wedge\wedge}P < 0.01$, $^{\wedge\wedge\wedge}P < 0.001$ vs. HFD-SHR rats. FOV: field of view

and HFD showed a cumulative effect. In a previous study, salt-loaded SHR/SP rats exhibited WM alterations that were resolved following antihypertensive treatment or by reducing cerebral perfusion through occlusion of the common carotid artery. The conditions induced by salt loading are similar to those

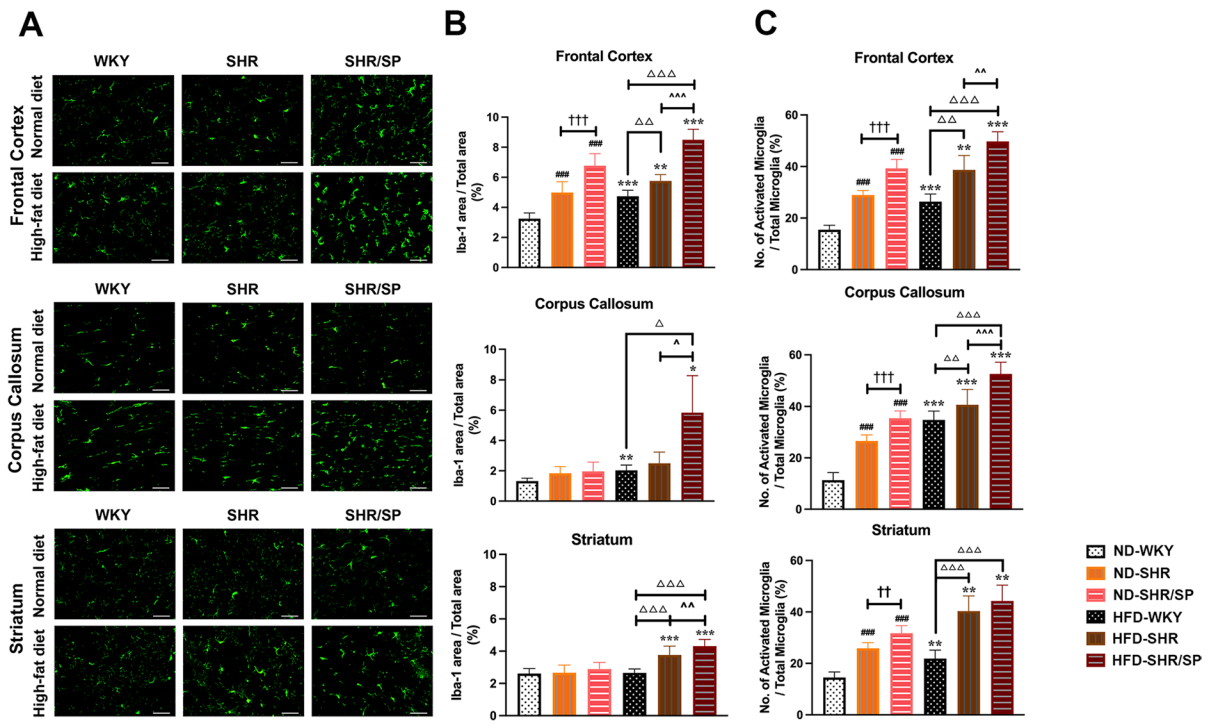

Fig. 7 HFD-induced microglia activation in the cerebral frontal cortex, corpus callosum, and striatum regions of WKY, SHR, and SHR/SP rats. **A** Representative photographs of Iba-1 immunostaining in the frontal cortex, corpus callosum, and striatum regions of WKY, SHR, and SHR/SP rats fed ND or HFD. Scale bar = 50 μm. **B** and **C** Quantification of area coverage by a positive Iba-1 signal, presented as a percentage of the total FOV area, and the percentage of activated microglia relative to the total microglia in the FOV in the frontal cortex, corpus callosum, and striatum regions. In the ND groups, both the number of activated microglia and the area of Iba-1-positive cells were significantly higher in ND-SHR and ND-SHR/SP rats across all regions compared to ND-WKY rats. Similar trends were observed in all regions of the HFD groups, with HFD-WKY, HFD-SHR, and HFD-SHR/SP rats displaying varying degrees of increase. The HFD groups exhibited a significant increase in all regions compared to their respective ND groups. Results are means ± SD (n = 3, 3 FOV for each region). $^{*}P<0.05$, $^{**}P<0.01$, $^{***}P<0.001$ vs. the corresponding results of the ND group. In the ND-fed group, $^{\#\#\#}P<0.001$ vs. the ND-WKY rats. In the ND-fed group, $^{\dagger\dagger}P<0.01$, $^{\dagger\dagger\dagger}P<0.001$ vs. the ND-SHR rats. In the HFD-fed group, $^{\Delta\Delta}P<0.01$, $^{\Delta\Delta\Delta}P<0.001$ vs. the HFD-WKY rats. In the HFD-fed group, $^{\wedge}P<0.05$, $^{\wedge\wedge}P<0.01$, $^{\wedge\wedge\wedge}P<0.001$ vs. HFD-SHR rats. FOV: field of view

observed in malignant hypertension in the SHR/SP rats' model. Consequently, the authors proposed that SHR/SP rats could serve as a model for posterior reversible encephalopathy syndrome [26]. However, in our study, when hypertensive SHR and SHR/SP rats were exposed to HFD, their blood pressure remained relatively unchanged, whereas WKY rats exhibited an increase. Combined with our MRI results, this suggested that the HFD-fed SHR/SP rat model effectively mimics CSVD. Additionally, an increase in blood pressure observed solely in WKY rats after HFD feeding implied that diet-induced alterations in blood pressure regulation may differ between hypertensive and normotensive rats. This underscores the intricate interplay between genetic predisposition and dietary influences. Not only the blood pressure, but genetic factors impact the body weight changes as well. As a result of the HFD, a notable increase in body weight was observed in all rat strains. However, the rate of body weight increase in SHR/SP rats was comparatively slower than that in WKY and SHR rats. This divergence in the dynamics of body weight suggested potential genetic factors in metabolic responses to the HFD, warranting further investigation.

In this study, analysis of vessels revealed that the density among the rat strains was similar, particularly in the corpus callosum region. These

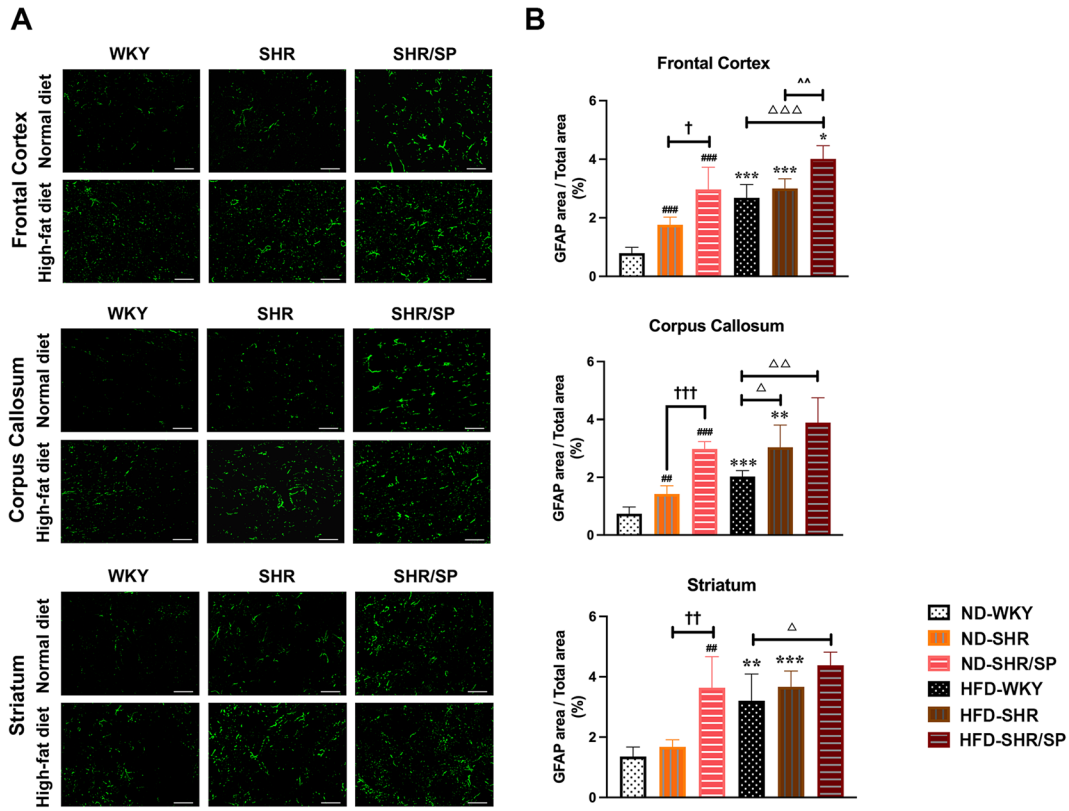

Fig. 8 HFD-induced astrocytosis in the cerebral frontal cortex, corpus callosum, and striatum regions of WKY, SHR, and SHR/SP rats. **A** GFAP immunostaining in the frontal cortex, corpus callosum, and striatum regions of WKY, SHR, and SHR/SP rats fed ND or HFD. Scale bar = 50 µm. **B** The graphs showed the area coverage by a positive GFAP signal, presented as a percentage of the total FOV area, in the frontal cortex, corpus callosum, and striatum regions. In the ND groups, the area of GFAP-positive cell counts were significantly higher in ND-SHR and ND-SHR/SP rats across all regions compared to ND-WKY rats. Similar trends were observed in all regions of the HFD groups, with HFD-WKY, HFD-SHR, and HFD-SHR/SP rats showing varying degrees of increase. The HFD groups exhibited a significant increase compared to their respective ND groups. Results are means ± SD (n = 3, 3 FOV for each region). $^{*}P<0.05$, $^{**}P<0.01$, $^{***}P<0.001$ vs. the corresponding results of the ND group. In the ND-fed group, $^{\#\#}P<0.01$, $^{\#\#\#}P<0.001$ vs. the ND-WKY rats. In the ND-fed group, $^{\dagger}P<0.05$, $^{\dagger\dagger}P<0.01$, $^{\dagger\dagger\dagger}P<0.001$ vs. the ND-SHR rats. In the HFD-fed group, $^{\Delta}P<0.05$, $^{\Delta\Delta}P<0.01$, $^{\Delta\Delta\Delta}P<0.001$ vs. the HFD-WKY rats. In the HFD-fed group, $^{\wedge\wedge}P<0.01$ vs. HFD-SHR rats. FOV: field of view

results align closely with those of a previous study [39]. Importantly, the density increased only in the frontal cortex region of all rat strains due to HFD, indicating the presence of an angiogenic signal specific to this region. Our study aligns with the findings of Adviye Ergul, where models of type 2 diabetes, such as Goto-Kakizaki (GK) rats and Lepr$^{db/db}$ mice, exhibited increased vessel density [40, 41]. Our results particularly emphasized the regional specificity of angiogenic responses to dietary factors and reinforce the intricate interplay between metabolism and cerebrovascular remodeling. HIF-1α, an angiogenic and inflammatory transcription factor, increased significantly across all regions in WKY, SHR, and SHR/SP rats when fed with HFD without affecting vessel number except frontal cortex region, suggesting the role of its angiogenesis function in this case may not be important. However, the possibility of the presence of pathological angiogenesis in those areas could not be ignored, as it is frequently observed in inflammatory conditions, and HFD is known to induce vessel inflammation. Angiogenesis is a complex process requiring sophisticated coordination between proangiogenic and vessel-stabilizing signals. Inflammatory conditions often lack such

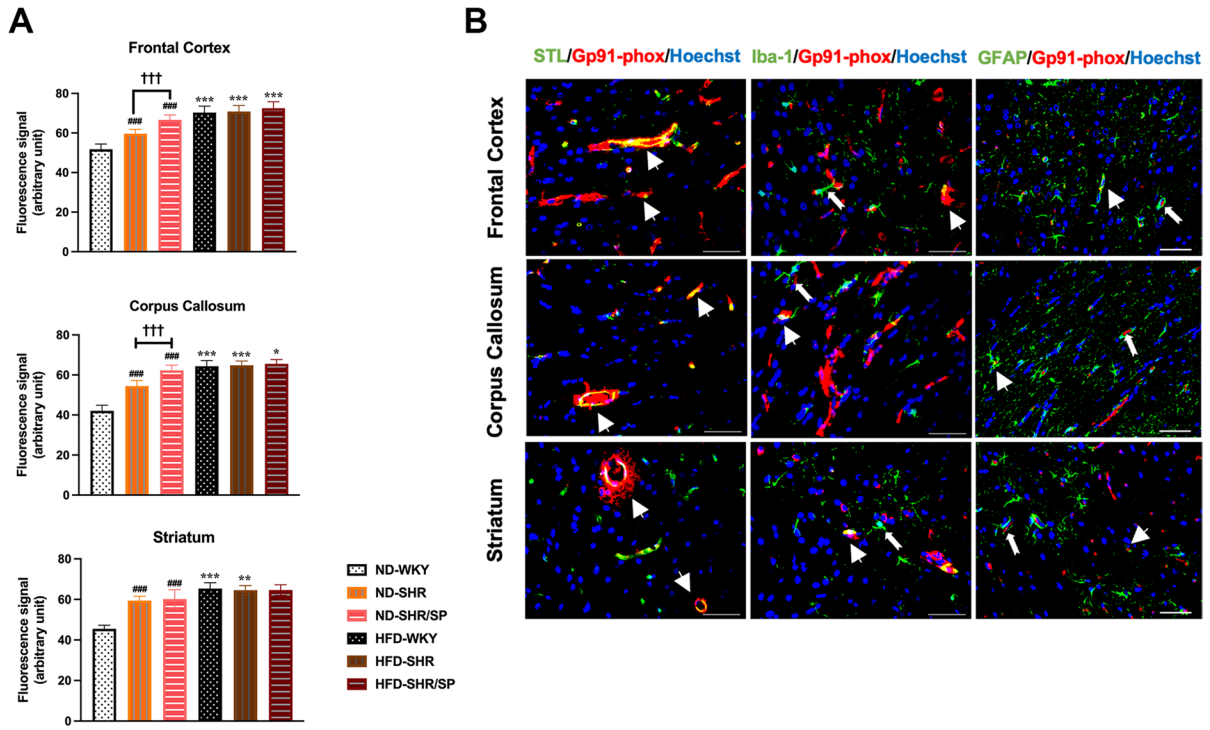

Fig. 9 HFD-induced expression of Gp91-phox in the WKY, SHR, and SHR/SP rats and its localization in the frontal cortex, corpus callosum, and striatum regions of HFD-SHR/SP rats. **A** Statistical analysis results of Gp91-phox expression were shown in the frontal cortex, corpus callosum, and striatum. HFD-induced expression of Gp91-phox in the frontal cortex, corpus callosum, and striatum regions of the brain of WKY, SHR, and SHR/SP rats. Results are means ± SD (n = 3, 3 FOV for each region). $^{*}P < 0.05$, $^{**}P < 0.01$, $^{***}P < 0.001$ vs. the corresponding results of the ND group. In the ND-fed group, $^{\#\#\#}P < 0.001$ vs. the ND-WKY rats. In the ND-fed group, $^{\dagger\dagger\dagger}P < 0.001$ vs. the ND-SHR rats. FOV: field of view. **B** The co-localization of Gp91-phox was shown in the frontal cortex, corpus callosum, and striatum regions of HFD-SHR/SP rats. The figure illustrated triple immunostaining for the vessel marker STL, microglia marker Iba-1, and astrocyte marker GFAP (green), oxidative stress marker Gp91-phox (red), and nuclei were identified using Hoechst (blue) in the frontal cortex, corpus callosum, and striatum regions of HFD-SHR/SP rats. Triple-stained merged photographs are shown here. Scale bar = 50 μm. Dovetail arrows show Iba-1 and GFAP expression surrounding Gp91-phox, whereas thick arrows represent Gp91-phox expression in STL, Iba-1, and GFAP

coordination, leading to a pathological type of angiogenesis, characterized by leaky vessels, which was observed in our study. Furthermore, in our study, the increase in neuroinflammatory glial cell number was most pronounced in HFD-fed SHR/SP rats, coinciding with increased vessel leakage. This suggested the existence of inflammation-mediated pathological angiogenesis in hypertensive conditions, which is exacerbated by HFD. While we did not investigate the precise cause of the increased HIF-1α, it is possible that hypoperfusion-induced hypoxia contributes to this phenomenon, given that both hypertension and HFD-induced metabolic changes are known to potentially lead to vessel alterations, resulting in hypoperfusion. Additionally, HIF-1α can also be induced by inflammatory signals such as IL-1β, where oxidative stress plays a crucial role [42].

Previous studies have reported that HIF-1α-mediated angiogenic signals and inflammation have the capacity to decrease the expression of BBB proteins including claudin 5 by increasing VEGF and matrix metalloproteinase levels [43, 44]. Also, VEGF expression is directly regulated by HIF-1α [45]. In our study, we found that HIF-1α is not only localized in blood vessels but is also localized in neuroinflammatory markers and activated neuroinflammatory markers surrounding HIF-1α. This finding suggested that hypoxia may play a role in the development of neuroinflammation. Meanwhile, we also found that

neuroinflammatory microglia and astrocytes were increased by hypertension, which is known to express matrix metalloproteinases in inflammatory conditions. Moreover, the introduction of an HFD further increased these factors. However, the hypertension-mediated increase of these factors might be sufficient for the reduction of BBB proteins such as claudin 5. Therefore, in the SHR/SP rats, HFD-mediated increased inflammation shows a minimal effect. Since there were almost no changes in the levels of these factors of CSVD pathology in normotensive WKY rats, the most significant increase in the changes in each of the CSVD pathology factors was observed after feeding the HFD, which led to a decrease in claudin 5 and a disruption of BBB integrity.

Hypertension has been known to induce the remodeling of small vessel basement membranes, leading to excessive deposition of collagens and fibronectin, resulting in fibrotic changes [46, 47]. However, our study has shown that the levels of basement membrane protein collagen IV remained similar in normotensive ND-fed WKY, hypertensive SHR, and SHR/SP rats. These findings are consistent with our other observations, including pathological and MRI changes in the WM, which were less pronounced in ND-fed hypertensive rats compared to their HFD counterparts. Hence, based on our study, it appears that hypertension alone may not suffice to induce changes in basement membranes within a 20-week timeframe, and a longer duration of hypertension exposure might be necessary to cause basement membrane changes. However, in HFD-fed normotensive WKY, we observed an increase in collagen IV levels, suggesting that HFD alone can induce collagen IV expression. However, when hypertensive rats were subjected to an HFD, collagen IV levels increased across all regions, and this increase was more substantial than that observed in WKY. These results suggested that while hypertension alone may not significantly alter collagen IV expression within our experimental timeframe, combining it with an HFD has a synergistic effect, resulting in a greater increase in collagen IV. Meanwhile, in our results on HIF-1α localization, we found that its increase was particularly pronounced mainly in the vasculature, which may contribute to one of the causes of remodeling of the vascular basement membrane [48]. Another possibility is attributable to the modulation of TGF-β expression by hypertension and HFD. Both hypertension and HFD have been shown to increase TGF-β expression in rodent kidneys, and the role of TGF-β in inducing collagen IV expression has been well-known [49].

ROS plays an important role in the homeostasis of the blood vessel wall, which may be part of the mechanism leading to the occurrence of CSVD. The most representative source of ROS is NADPH oxidase (NOX) and the NOX2 is the main source of ROS production in humans. Here, at the end of this study, we observed the effect of HFD combined with hypertension on oxidative stress NOX2 marker Gp91-phox. Many previous studies have confirmed that long-term hypertension in experimental animals and human brains can produce adverse effects such as inflammation and oxidative stress [50]. In our results, we also observed an increase in the Gp91-phox expression in the hypertensive SHR and SHR/SP rats. Combined with our other research results, this mechanism may be that hypertension may increase the permeability of blood vessel walls, promote the entry of inflammatory substances into brain tissue, and increase the generation of oxidative stress. Moreover, oxidative stress then aggravates cerebrovascular damage and inflammation, resulting in sustained adverse effects on cerebrovascular integrity.

Next, we focused on the changes in oxidative stress in hypertensive rats and normotensive rats after HFD. The effects of HFD on hypertensive rat strains were modest, while in normotensive WKY rats, it demonstrated an inducing effect. This result suggested that similar to claudin 5, hypertension may already increase Gp91-phox levels to a point where further increase becomes difficult. Also, previous studies showed that NADPH oxidase activity/expression is increased in laboratory animals given HFD [51–53], and further indicate that diet-induced NADPH oxidase activity mediates obesity-related cytokine/chemokine release as well as insulin resistance, hyperlipidemia, and liver steatosis [53]. These results implied that HFD, as an independent risk factor, produces oxidative stress in the brain. Moreover, especially in the severely hypertensive SHR/SP rats, we observed that oxidative stress marker was more expressed in blood small vessels and was also expressed in neuroinflammatory markers. Furthermore, activated neuroinflammatory markers were also observed around oxidative stress markers. This suggested that HFD can aggravate and increase

oxidative stress in the cerebral small blood vessels of severely hypertensive rats, continue to increase vascular permeability, and produce severe vascular leakage, thereby activating neuroinflammatory molecules around small blood vessels. The sustained inflammatory pathway will also increase ROS and increase oxidative stress, which may cause severe damage to the BBB. Taken together, our findings speculated that neuroinflammation and oxidative stress are both triggered by and the result of vascular injury. Thus, the discovery of this complex relationship between neuroinflammation and oxidative stress helped us to reveal one of the mechanisms involved in the superimposed pathological effects of hypertension combined with HFD on CSVD.

There are also several limitations that need to be recognized. Although we have initially revealed that the possible mechanisms of vascular leakage exacerbated by a high-fat diet are perivascular inflammation and increased oxidative stress and hypoxic factors in the vasculature, we have not explored in depth the molecular mechanisms underlying the increased oxidative stress, hypoxic factors, and inflammation, and we have not clarified which specific signaling pathways contribute to the changes that occur. In addition, the reasons for the differential pathologic changes in different regions of the brain were not elucidated in this study. These are noteworthy limitations, and future research efforts will aim to explore in greater depth the molecular complexities involved in oxidative stress, hypoxia, and inflammation, as well as to understand regional differences in brain pathology.

In conclusion, our study demonstrated that HFD and hypertension can induce and synergize a variety of responses including neuroinflammation, oxidative stress, and angiogenic/hypoxia signals within the cerebral small vasculature and surrounding cellular environment. Such findings contribute to a better understanding of the complex interplay between metabolic factors and hypertensive conditions in maintaining cerebrovascular and white matter health and help to formulate improved therapeutic management for multiple risk factors induced CSVD.

Acknowledgements We would like to acknowledge the technical expertise of the Interdisciplinary Center for Science Research, Organization for Research and Academic Information, and Department of Experimental Animals, Interdisciplinary Center for Science Research, Shimane University. We would also like to thank Yasuko Wada, Abul Kalam Azad, Yuxin Liu, Xinlang Liu, and Pang Bo for their technical support during the experiments.

Author contributions **Yuchi Zhang**: Conceptualization, Data curation, Methodology, Writing – original draft. **Abdullah Md. Sheikh**: Conceptualization, Methodology, Writing – review & editing. **Shatera Tabassum**: Methodology, Supervision, Validation. **Kenichi Iwasa**: Supervision, Validation. **Abu Zaffar Shibly**: Methodology, Supervision. **Xiaojing Zhou**: Validation. **Ruochen Wang**: Validation. **Jubo Bhuiya**: Methodology, Validation. **Abdullah Fatema Binte**: Validation. **Shozo Yano**: Validation. **Yoshihito Aoki:** Validation. **Atsushi Nagai**: Conceptualization, Project administration, Supervision, Writing – review & editing. All authors provided critical feedback and contributed to the final manuscript.

Funding This research did not receive any specific grant from funding agencies in the public, commercial, or not-for-profit sectors.

Data Availability The data that support the findings of this study are available upon request from the authors.

Declarations

Ethics approval All animals were used according to the ARRIVE reporting guidelines (Animal Research: Reporting of In Vivo Experiments), and guidelines of the Institute of Experimental Animals of Shimane University. The experimental protocols and procedures were approved by the Ethical Committee of Shimane University (approval code: IZ2-96).

Conflict of interest The authors declare that they have no conflicts of interest with the contents of this manuscript.

References

1. Chojdak-Łukasiewicz J, Dziadkowiak E, Zimny A, Paradowski B. Cerebral small vessel disease: A review. Adv Clin Exp Med. 2021;30(3):349–56. https://doi.org/10.17219/acem/131216.
2. Cuadrado-Godia E, Dwivedi P, Sharma S, Ois Santiago A, Roquer Gonzalez J, Balcells M, Laird J, Turk M, Suri HS, Nicolaides A, Saba L, Khanna NN, Suri JS. Cerebral Small Vessel Disease: A Review Focusing on Pathophysiology, Biomarkers, and Machine Learning Strategies. J Stroke. 2018;20(3):302–20. https://doi.org/10.5853/jos.2017.02922.
3. Li Q, Yang Y, Reis C, Tao T, Li W, Li X, Zhang JH. Cerebral Small Vessel Disease. Cell Transplant. 2018;27(12):1711–22. https://doi.org/10.1177/0963689718795148.
4. Lee WJ, Chou KH, Lee PL, Peng LN, Wang PN, Lin CP, Chen LK, Chung CP. Cerebral small vessel disease phenotype and 5-year mortality in asymptomatic middle-to-old aged individuals. Sci Rep. 2021;11(1):23149. https://doi.org/10.1038/s41598-021-02656-7.

5. Rensma SP, van Sloten TT, Launer LJ, Stehouwer CDA. Cerebral small vessel disease and risk of incident stroke, dementia and depression, and all-cause mortality: A systematic review and meta-analysis. Neurosci Biobehav Rev. 2018;90:164–73. https://doi.org/10.1016/j.neubiorev.2018.04.00.
6. Ihara M, Yamamoto Y. Emerging Evidence for Pathogenesis of Sporadic Cerebral Small Vessel Disease. Stroke. 2016;47(2):554–60. https://doi.org/10.1161/STROKEAHA.115.009627.
7. Heye AK, Thrippleton MJ, Chappell FM, Hernández Mdel C, Armitage PA, Makin SD, Maniega SM, Sakka E, Flatman PW, Dennis MS, Wardlaw JM. Blood pressure and sodium: Association with MRI markers in cerebral small vessel disease. J Cereb Blood Flow Metab. 2016;36(1):264–74. https://doi.org/10.1038/jcbfm.2015.64.
8. Wang Z, Chen Q, Chen J, Yang N, Zheng K. Risk factors of cerebral small vessel disease: A systematic review and meta-analysis. Medicine (Baltimore). 2021;100(51):e28229. https://doi.org/10.1097/MD.0000000000028229.
9. Inoue Y, Shue F, Bu G, Kanekiyo T. Pathophysiology and probable etiology of cerebral small vessel disease in vascular dementia and Alzheimer's disease. Mol Neurodegener. 2023;18(1):46. https://doi.org/10.1186/s13024-023-00640-5.
10. Marini S, Anderson CD, Rosand J. Genetics of Cerebral Small Vessel Disease. Stroke. 2020;51(1):12–20. https://doi.org/10.1161/STROKEAHA.119.024151.
11. Bai T, Yu S, Feng J. Advances in the Role of Endothelial Cells in Cerebral Small Vessel Disease. Front Neurol. 2022;13: 861714. https://doi.org/10.3389/fneur.2022.861714.
12. Rajeev V, Fann DY, Dinh QN, Kim HA, De Silva TM, Lai MKP, Chen CL, Drummond GR, Sobey CG, Arumugam TV. Pathophysiology of blood brain barrier dysfunction during chronic cerebral hypoperfusion in vascular cognitive impairment. Theranostics. 2022;12(4):1639–58. https://doi.org/10.7150/thno.68304.
13. Ohtsuki S, Yamaguchi H, Katsukura Y, Asashima T, Terasaki T. mRNA expression levels of tight junction protein genes in mouse brain capillary endothelial cells highly purified by magnetic cell sorting. J Neurochem. 2008;104(1):147–54. https://doi.org/10.1111/j.1471-4159.2007.05008.x.
14. Dearborn JL, Schneider AL, Sharrett AR, Mosley TH, Bezerra DC, Knopman DS, Selvin E, Jack CR, Coker LH, Alonso A, Wagenknecht LE, Windham BG, Gottesman RF. Obesity, Insulin Resistance, and Incident Small Vessel Disease on Magnetic Resonance Imaging: Atherosclerosis Risk in Communities Study. Stroke. 2015;46(11):3131–6. https://doi.org/10.1161/STROKEAHA.115.010060.
15. Tb M, G, T., A, G., D, A. Erratum to "Suffering from Cerebral Small Vessel Disease with and without Metabolic Syndrome." Open Med (Wars). 2020;16(1):23. https://doi.org/10.1515/med-2021-0006.
16. Nassir CMNCM, Ghazali MM, Hashim S, Idris NS, Yuen LS, Hui WJ, Norman HH, Gau CH, Jayabalan N, Na Y, Feng L, Ong LK, Abdul Hamid H, Ahamed HN, Mustapha M. Diets and Cellular-Derived Microparticles: Weighing a Plausible Link With Cerebral Small Vessel Disease. Front Cardiovasc Med. 2021;8:632131. https://doi.org/10.3389/fcvm.2021.632131.
17. Chen YC, Lu BZ, Shu YC, Sun YT. Spatiotemporal Dynamics of Cerebral Vascular Permeability in Type 2 Diabetes-Related Cerebral Microangiopathy. Front Endocrinol (Lausanne). 2022;12: 805637. https://doi.org/10.3389/fendo.2021.805637.
18. Attuquayefio T, Stevenson RJ, Oaten MJ, Francis HM. A four-day Western-style dietary intervention causes reductions in hippocampal-dependent learning and memory and interoceptive sensitivity. PLoS ONE. 2017;12(2):e0172645. https://doi.org/10.1371/journal.pone.0172645.
19. Clemente-Suárez VJ, Beltrán-Velasco AI, Redondo-Flórez L, Martín-Rodríguez A, Tornero-Aguilera JF. Global Impacts of Western Diet and Its Effects on Metabolism and Health: A Narrative Review. Nutrients. 2023;15(12):2749. https://doi.org/10.3390/nu15122749.
20. Mustapha M, Nassir CMNCM, Aminuddin N, Safri AA, Ghazali MM. Cerebral Small Vessel Disease (CSVD) - Lessons From the Animal Models. Front Physiol. 2019;10:1317. https://doi.org/10.3389/fphys.2019.01317.
21. Olivera, S., Graham, D. Sex differences in preclinical models of hypertension. J Hum Hypertens, 2022. 1–7. https://doi.org/10.1038/s41371-022-00770-1
22. Yamori Y, Horie R, Sato M, Ohta K. Proceedings: Prophylactic trials for stroke in stroke-prone SHR: effect of sex hormones. Jpn Heart J. 1976;17(3):404–6. https://doi.org/10.1536/ihj.17.404.
23. Tochinai R, Sekizawa S, Kobayashi I, Kuwahara HM. Autonomic nervous activity in rats can be evaluated by blood photoplethysmography-derived pulse rate variability analysis. Transl Regul Sci. 2021;3(1):17–21. https://doi.org/10.33611/trs.2021-001.
24. Kuwahara M, Sugano S, Yayou K, Tsubone H, Kobayashi H. Evaluation of a new tail-cuff method for blood pressure measurements in rats with special reference to the effects of ambient temperature. Jikken Dobutsu. 1991;40(3):331–6. https://doi.org/10.1538/expanim1978.40.3_331.
25. Sasaki K, Yoshizaki F. Investigation into hippocampal nerve cell damage through the mineralocorticoid receptor in mice. Mol Med Rep. 2015;12(5):7211–20. https://doi.org/10.3892/mmr.2015.4406.
26. Herisson F, Zhou I, Mawet J, Du E, Barfejani AH, Qin T, Cipolla MJ, Sun PZ, Rost NS, Ayata C. Posterior reversible encephalopathy syndrome in stroke-prone spontaneously hypertensive rats on high-salt diet. J Cereb Blood Flow Metab. 2019;39(7):1232–46. https://doi.org/10.1177/0271678X17752795.
27. Azad AK, Sheikh AM, Haque MA, Osago H, Sakai H, Shibly AZ, Yano S, Michikawa M, Hossain S, Tabassum S, Zhou AG, Zhang X, Nagai YA. Time-Dependent Analysis of Plasmalogens in the Hippocampus of an Alzheimer's Disease Mouse Model: A Role of Ethanolamine Plasmalogen. Brain Sci. 2021;11(12):1603. https://doi.org/10.3390/brainsci11121603.
28. Shibly AZ, Sheikh AM, Michikawa M, Tabassum S, Azad AK, Zhou X, Zhang Y, Yano S, Nagai A. Analysis of Cerebral Small Vessel Changes in AD Model Mice. Biomedicines. 2022;11(1):50. https://doi.org/10.3390/biomedicines11010050.

29. Weiss HR, Buchweitz E, Murtha TJ, Auletta M. Quantitative regional determination of morphometric indices of the total and perfused capillary network in the rat brain. Circ Res. 1982;51(4):494–503. https://doi.org/10.1161/01.RES.51.4.494.
30. Saubaméa B, Cochois-Guégan V, Cisternino S, Scherrmann JM. Heterogeneity in the rat brain vasculature revealed by quantitative confocal analysis of endothelial barrier antigen and P-glycoprotein expression. J Cereb Blood Flow Metab. 2012;32(1):81–92. https://doi.org/10.1038/jcbfm.2011.109.
31. Lee SP, Duong TQ, Yang G, Iadecola C, Kim SG. Relative changes of cerebral arterial and venous blood volumes during increased cerebral blood flow: implications for BOLD fMRI. Magn Reson Med. 2001;45(5):791–800. https://doi.org/10.1002/mrm.1107.
32. Elabi OF, Cunha JPMCM, Gaceb A, Fex M, Paul G. High-fat diet-induced diabetes leads to vascular alterations, pericyte reduction, and perivascular depletion of microglia in a 6-OHDA toxin model of Parkinson disease. J Neuroinflammation. 2021;18(1):175. https://doi.org/10.1186/s12974-021-02218-8.
33. Tabitha Green. (2019). Shape-shifting Brain Cells. ASU - Ask A Biologist. Retrieved January 8, 2024 from https://askabiologist.asu.edu/plosable/shape-shifting-brain-cells.
34. Arba F, Leigh R, Inzitari D, Warach SJ, Luby M, Lees KR. Blood–brain barrier leakage increases with small vessel disease in acute ischemic stroke. Neurol. 2017;89(21):2143–50. https://doi.org/10.1212/WNL.0000000000004677.
35. Lai Y, Jiang C, Du X, Sang C, Guo X, Bai R, Tang R, Dong J, Ma C. Effect of intensive blood pressure control on the prevention of white matter hyperintensity: systematic review and meta-analysis of randomized trials. J Clin Hypertens (Greenwich). 2020;22(11):1968–73. https://doi.org/10.1111/jch.14030.
36. Giezendanner S, Fisler MS, Soravia LM, Andreotti J, Walther S, Wiest R, Dierks T, Federspiel A. Microstructure and cerebral blood flow within white matter of the human brain: a TBSS analysis. PLoS ONE. 2016;11(3):e0150657. https://doi.org/10.1371/journal.pone.0150657.
37. Ritz MF, Grond-Ginsbach C, Kloss M, Tolnay M, Fluri F, Bonati H, Traenka L, Zeis C, Schaeren-Wiemers T, Peters N, Engelter N, Engelter ST, Alexandre Lyrer P. Identification of inflammatory, metabolic, and cell survival pathways contributing to cerebral small vessel disease by postmortem gene expression microarray. Curr Neurovasc Res. 2016;13(1):58–67. https://doi.org/10.2174/1567202612666151027151025.
38. Murray ME, Vemuri P, Preboske GM, Murphy MC, Schweitzer KJ, Parisi JE, Jack CR Jr, Dickson DW. A quantitative postmortem MRI design sensitive to white matter hyperintensity differences and their relationship with underlying pathology. Neuropathol Exp Neurol. 2012;71(12):1113–22. https://doi.org/10.1097/NEN.0b013e318277387e.
39. Ritz MF, Fluri F, Engelter ST, Schaeren-Wiemers N, Lyrer PA. Cortical and putamen age-related changes in the microvessel density and astrocyte deficiency in spontaneously hypertensive and stroke-prone spontaneously hypertensive rats. Curr Neurovasc Res. 2009;6(4):279–87. https://doi.org/10.2174/156720209789630311.
40. Li W, Prakash R, Kelly-Cobbs AI, Ogbi S, Kozak A, El-Remessy AB, Schreihofer DA, Fagan SC, Ergul A. Adaptive cerebral neovascularization in a model of type 2 diabetes: relevance to focal cerebral ischemia. Diabetes. 2010;59(1):228–35. https://doi.org/10.2337/db09-0902.
41. Prakash R, Johnson M, Fagan SC, Ergul A. Cerebral neovascularization and remodeling patterns in two different models of type 2 diabetes. PLoS ONE. 2013;8(2): e56264. https://doi.org/10.1371/journal.pone.0056264.
42. Zhang, H., Xu, R., Wang, Z., Contribution of oxidative stress to HIF-1-mediated profibrotic changes during the kidney damage. Oxid Med Cell Longev. 2021, 6114132. https://doi.org/10.1155/2021/6114132
43. Cao Y, Li Z, Li H, Ni C, Li L, Yang N, Shi C, Zhong Y, Cui D, Guo X. Hypoxia-inducible factor-1α is involved in isoflurane-induced blood-brain barrier disruption in aged rats model of POCD. Behav Brain Res. 2018;339:39–46. https://doi.org/10.1016/j.bbr.2017.09.004.
44. Argaw AT, Gurfein BT, Zhang Y, Zameer A, John GR. VEGF-mediated disruption of endothelial CLN-5 promotes blood-brain barrier breakdown. Proc Natl Acad Sci U S A. 2009;106(6):1977–82. https://doi.org/10.1073/pnas.080869810.
45. Terashima J, Sampei S, Iidzuka M, Ohsakama A, Tachikawa C, Satoh J, Kudo K, Habano W, Ozawa S. VEGF expression is regulated by HIF-1α and ARNT in 3D KYSE-70, esophageal cancer cell spheroids. Cell Biol Int. 2016;40(11):1187–94. https://doi.org/10.1002/cbin.10656.
46. Barallobre-Barreiro J, Loeys B, Mayr M, Rienks M, Verstraeten A, Kovacic JC. Extracellular matrix in vascular disease, part 2/4: JACC Focus Seminar. J Am Coll Cardiol. 2020;75(17):2189–203. https://doi.org/10.1016/j.jacc.2020.03.018.
47. Martinez-Quinones P, McCarthy CG, Watts SW, Klee NS, Komic A, Calmasini FB, Priviero F, Warner A, Chenghao Y, Wenceslau CF. Hypertension induced morphological and physiological changes in cells of the arterial wall. Am J Hypertens. 2018;31(10):1067–78. https://doi.org/10.1093/ajh/hpy083.
48. Gilkes DM, Bajpai S, Chaturvedi P, Wirtz D, Semenza GL. Hypoxia-inducible factor 1 (HIF-1) promotes extracellular matrix remodeling under hypoxic conditions by inducing P4HA1, P4HA2, and PLOD2 expression in fibroblasts. J Biol Chem. 2013;288(15):10819–29. https://doi.org/10.1074/jbc.M112.442939.
49. Iglesias-de la Cruz MC, Ziyadeh FN, Isono M, Kouahou M, Han DC, Kalluri R, Mundel P, Chen S. Effects of high glucose and TGF-beta1 on the expression of collagen IV and vascular endothelial growth factor in mouse podocytes. Kidney Int. 2002;62(3):901–13. https://doi.org/10.1046/j.1523-1755.2002.00528.x.
50. Barrows IR, Ramezani A, Raj DS. Inflammation, immunity, and oxidative stress in hypertension-partners in crime? Adv Chronic Kidney Dis. 2019;26(2):122–30. https://doi.org/10.1053/j.ackd.2019.03.001.
51. Bruce-Keller AJ, White CL, Gupta S, Knight AG, Pistell PJ, Ingram DK, Morrison CD, Keller JN. NOX activity in brain aging: exacerbation by high fat diet. Free Radic Biol Med. 2010;49(1):22–30. https://doi.org/10.1016/j.freeradbiomed.2010.03.006.

52. Furukawa S, Fujita T, Shimabukuro M, Iwaki M, Yamada Y, Nakajima Y, Nakayama O, Makishima M, Matsuda M, Shimomura I. Increased oxidative stress in obesity and its impact on metabolic syndrome. J Clin Invest. 2017;114(12):1752–61. https://doi.org/10.1172/JCI21625.
53. Pepping JK, Vandanmagsar B, Fernandez-Kim SO, Zhang J, Mynatt RL, Bruce-Keller AJ. Myeloid-specific deletion of NOX2 prevents the metabolic and neurologic consequences of high fat diet. PLoS ONE. 2017;12(8): e0181500. https://doi.org/10.1371/journal.pone.0181500.